WDHD1 is essential for the survival of PTEN-inactive triple negative breast cancer

Ayse Ertay[1], Huiquan Liu[2], Dian Liu[2], Ping Peng[2], Charlotte Hill[1], Hua Xiong[2], David Hancock[3], Xianglin Yuan[2], Marcin R. Przewloka[1,4], Mark Coldwell[1,4], Michael Howell[5], Paul Skipp[1,4,6], Rob M. Ewing[1,4], Julian Downward[3,*] and Yihua Wang[1,4,7,*]

[1]Biological Sciences, Faculty of Environmental and Life Sciences, University of Southampton, Southampton SO17 1BJ, UK; [2]Department of Oncology, Tongji Hospital, Tongji Medical College, Huazhong University of Science and Technology, Wuhan 430030, China; [3]Oncogene Biology, The Francis Crick Institute, London NW1 1AT, UK; [4]Institute for Life Sciences, University of Southampton, Southampton, SO17 1BJ, UK; [5]High-Throughput Screening, The Francis Crick Institute, London NW1 1AT, UK; [6]Centre for Proteomic Research, Institute for Life Sciences, University of Southampton, Southampton, SO17 1BJ, UK; [7]NIHR Southampton Biomedical Research Centre, University Hospital Southampton SO16 6YD, UK.

*Correspondence should be addressed to JD (e-mail: Julian.Downward@crick.ac.uk) or YW (e-mail: yihua.wang@soton.ac.uk).

Keywords

WDHD1, triple negative breast cancer, PTEN, siRNA screen, TCGA, protein translation

Running title

WDHD1 in TNBC

Abstract

Triple negative breast cancer (TNBC) is the most aggressive type of breast cancer that lacks the oestrogen receptor, progesterone receptor and human epidermal growth factor receptor 2, making it difficult to target therapeutically. Targeting synthetic lethality is an alternative approach for cancer treatment. TNBC shows frequent loss of phosphatase and tensin homolog (PTEN) expression, which is associated with poor prognosis and treatment response. To identify PTEN synthetic lethal interactions, TCGA analysis coupled with a whole genome siRNA screen in isogenic PTEN negative and positive cells were performed. Among the candidate genes essential for the survival of PTEN-inactive TNBC cells, *WDHD1* (WD repeat and high-mobility group box DNA binding protein 1) expression was increased in the low *vs.* high *PTEN* TNBC samples. It was also the top hit in the siRNA screen and its knockdown significantly inhibited cell viability in PTEN negative cells, which was further validated in 2D and 3D cultures. Mechanistically, WDHD1 is important to mediate a high demand of protein translation in PTEN-inactive TNBC. Finally, the importance of WDHD1 in TNBC was confirmed in patient samples obtained from the TCGA and tissue microarrays with clinic-pathological information. Taken together, as an essential gene for the survival of PTEN-inactive TNBC cells, *WDHD1* could be a potential biomarker or a therapeutic target for TNBC.

Introduction

Breast cancer is the most common cancer type and the leading cause of cancer death in women worldwide[1]. Triple negative breast cancer (TNBC) lacks the oestrogen receptor (ER), progesterone receptor (PR) and human epidermal growth factor receptor 2 (HER2), and accounts for between 10% and 20% of breast cancers[2–5]. TNBC is the most aggressive and high-grade breast cancer type with high risk of tumour recurrence and metastasis compared to the other breast cancer subtypes[6]. As TNBC lacks all three receptors, this causes more challenges for the treatment of the disease. Chemotherapy has been the only standard treatment option to improve the overall survival rate of TNBC patients for several years[7]. Therefore, it is important to study gene profiling by identifying different gene expression signatures in TNBC to discover a novel biomarker or targeted therapy for the disease. Atezolizumab (TECENTRIQ®), an anti-programmed death-ligand 1 (PD-L1) monoclonal antibody (checkpoint inhibitor), was approved as the first breast cancer immunotherapy to be combined with chemotherapy (Abraxane; nab®-Paclitaxel) for PD-L1 positive TNBC[8]. As a heterogeneous disease[9], further gene profiling studies are required to identify novel biomarkers or therapeutic targets for TNBC.

TNBC shows frequent loss of phosphatase and tension homolog (PTEN) expression compared to the other molecular subtypes of breast cancer[10,11]. It has been shown that loss of PTEN expression was significantly associated with TNBC that shows poor prognosis and significant links with high-grade tumour, larger tumour size, lymph node metastasis and tumour recurrence[12]. PTEN was identified as a tumour suppressor gene, located on 10q23 chromosome band, which plays an essential role to control cell cycle, growth and survival[13]. Mechanistically, PTEN has a cytoplasmic lipid phosphatase role which can inhibit the

phosphatidylinositol 3-kinase (PI3K)-AKT pathway[13,14], and the nuclear phosphatase-independent role of PTEN which has been shown to maintain genomic stability[15,16].

Targeting synthetic lethality is an alternative approach for cancer treatment[17]. To identify novel targeted therapies, synthetic lethality screens were performed, including RNA interference (RNAi) screens[18,19]. One of the well-known examples of synthetic lethality interaction is between *BRCA1/2* and *PARP*. *BRCA1/2* are tumour suppressor genes that have a role in homologous-recombination-mediated DNA repair and *PARP* is involved in base excision repair. Tumours with *BRCA1/2* deficiency depend on *PARP1* for DNA repair. Thus, inhibition of PARP1 kills *BRCA1/2* deficient tumours[20,21]. Discovering PTEN synthetic lethal interactions in TNBC may provide potential biomarkers or targeted therapies for this breast cancer type that does not have successful treatment options.

In this study, candidate genes essential for the survival of PTEN-inactive TNBC cells were identified by the TCGA analysis and a whole genome siRNA screen in isogenic PTEN negative and positive cells. Among them, WD repeat and high-mobility group box DNA binding protein 1 (*WDHD1*) expression was increased in the low *vs.* high *PTEN* TNBC samples. It was also the top candidate gene whose knockdown significantly inhibited cell viability in PTEN negative cells, which was further validated in 2D and 3D cultures. Mechanistically, WDHD1 was important to mediate a high demand of protein translation in PTEN-inactive TNBC. Finally, the importance of WDHD1 in TNBC was confirmed in patient samples obtained from the TCGA and tissue microarrays with clinic-pathological information.

Results

TCGA analysis confirms PTEN expression is decreased in TNBC and correlates with clinical stages.

It has been stated that PTEN inactivation occurs more frequently in TNBC than the other subtypes of breast cancer[11,12]. To confirm this finding, clinical data of breast invasive carcinoma (TCGA, PanCancer) was obtained from cBioportal (https://www.cbioportal.org/). *PTEN,* mRNA levels were analysed in the normal breast samples and each molecular subtypes of breast cancer. *PTEN*, mRNA levels were significantly lower in TNBC compared to the normal breast, luminal A, luminal B and HER2+ subtypes, although PTEN mutation frequency was similar (~6%) across all subtypes of breast cancer (Fig. S1a; $P < 0.0001$).

Protein (RPPA) TCGA breast invasive carcinoma data from the UCSC Cancer Genome Browser (https://genome-cancer.ucsc.edu/) was obtained. The categorised TNBC samples (TCGA, Provisional) from the cBioportal website was aligned with protein (RPPA) data (see Supplementary Materials). A significant correlation between mRNA and protein levels of PTEN (Fig. S1b; $r = 0.55$; $P = 0.0001$) suggested that PTEN inactivation in TNBC occurs at the transcriptional level. The number of patients with T2 and above, or Stage II and above, in PTEN high TNBC samples was significantly lower than PTEN low group (Fig. S1c, d; $P < 0.05$). Functionally, decreased PTEN levels were responsible for the high AKT activity in TNBC, since there was a significant negative correlation between the levels of phosphorylated AKT (AKT1_PT308, a main downstream molecule of PTEN[22]) and PTEN in TNBC (Fig. S1e; $r = -0.55$; $P = 0.0001$).

These findings confirm that reduced PTEN levels correlate with advanced clinical stages and a high AKT activity in TNBC.

Candidate genes essential for the survival of PTEN-inactive TNBC cells are identified by the TCGA analysis and a whole genome siRNA screen.

As shown in Figure 1a, 92 TNBC samples were identified from TCGA. *PTEN,* mRNA expression was widely distributed across all TNBC samples, therefore the top 10% and bottom 10% of samples were defined as high and low *PTEN*, respectively. 3,009 mRNAs were identified as differentially expressed in the high *vs.* low *PTEN* groups (Fig. S1f; $P < 0.05$).

A whole genome siRNA screen was performed in isogenic GFP-labelled PTEN negative (PTEN-) cells and CherryFP-labelled PTEN positive (PTEN+) cells (Figs. S2 and S3a; details in Supplementary Materials). 4,647 genes were identified as showing differential effects on cell viability in PTEN- *vs.* PTEN+ cells (Fig. S3b; $P < 0.05$).

By cross-referencing TCGA analysis with the whole genome siRNA screen, 47 candidate genes essential for the survival of PTEN-inactive TNBC cells were identified (Fig. 1b, c; Table S1 and S2). Among them, *WDHD1* expression was increased in the low *vs.* high *PTEN* TNBC samples (Table S1; $P = 0.03$). It was also the top candidate gene whose knockdown significantly inhibited cell viability in PTEN negative cells (Z-score = -1.26) with mild effects on PTEN positive cells (Table S2; Z-score = -0.32; $P = 0.009$).

WDHD1 expression is affected by PTEN status in TNBC cells.

TCGA analysis suggested that *WDHD1* expression is increased in the low *vs.* high *PTEN* TNBC samples. To validate this finding, both protein and mRNA levels of WDHD1 were measured in a panel of TNBC cell lines, either PTEN WT (HCC1806, BT20, MDA-MB-157 and MDA-MB-231) or PTEN null (MDA-MB-468, HCC1395, HCC1937 and HCC38). We

found WDHD1 was highly expressed at both the protein (Fig. 2a, b; $P < 0.05$) and mRNA (Fig. 2c, d; $P < 0.01$) level in PTEN null *vs.* WT TNBC cell lines.

To further confirm the relationship between PTEN and WDHD1 expression levels, we introduced into MDA-MB-468 cells (PTEN null) a regulatable PTEN construct that is conditionally responsive to doxycycline (DOX). Addition of DOX induces PTEN expression in MDA-MB-468 cells expressing TR-PTEN (MDA-MB-468-TR-PTEN) to a similar level in a non-tumorigenic triple negative human breast epithelial cell line MCF10A (Fig. S2a). As shown in Figure 3, WDHD1 levels were significantly reduced upon PTEN expression (DOX+) in MDA-MB-468-TR-PTEN cells at both mRNA and protein levels, as demonstrated by the results from the western blot (Fig. 3a, b; $P < 0.01$), qRT-PCR (Fig. 3c; $P < 0.0001$) and immunofluorescence staining of WDHD1 (Fig. 3d).

Given our findings that decreased PTEN levels are responsible for the high AKT activity in TNBC, we then determined if AKT is involved in the regulation of WDHD1 expression in TNBC cells. An AKT inhibitor (AKT VIII) was used to treat PTEN null type TNBC cell lines MDA-MB-468 (Fig. 4a), HCC1395 (Fig. 4b), HCC1937 (Fig. 4c) and HCC38 (Fig. 4d). AKT activity, monitored by the levels of phosphorylated AKT (pAKT Thr308 and Ser473), was inhibited following the treatment with AKT VIII in all PTEN null type TNBC cell lines (Fig. 4a-d). Subsequently, WDHD1 levels were significantly reduced upon AKT inhibition in these cells (Fig. 4a-d; $P < 0.05$). The impact of PTEN-AKT signalling on WDHD1 expression was further confirmed by the TCGA analysis. To reflect the functional consequence of PTEN status, we decided to check p-AKT_308 levels and the correlation with *WDHD1* expression in TCGA. We demonstrated that there was a significant positive correlation between *WDHD1*, mRNA expression and pAKT_308 levels in the TCGA dataset (Fig. 4e; $r = 0.3321$, $P = 0.0296$).

Taken together, our results demonstrate that WDHD1 expression is affected by PTEN status in TNBC cells and this is mainly achieved by AKT signalling.

WDHD1 is required for the survival of PTEN null TNBC cells cultured in 2D or 3D.

The initial whole genome siRNA screen suggested that *WDHD1* depletion selectively inhibits cell viability in PTEN negative *vs.* positive TNBC cells. To validate this observation, *WDHD1* expression was down-regulated by 2 individual siRNA oligos in the aforementioned panel of TNBC cell lines and cell viability was measured by Cell-Titer Glo® assays (Fig. S4). Knockdown of *WDHD1* in PTEN WT TNBC cell lines (HCC1806, BT20, MDA-MB-157 and MDA-MB-231) showed mild, but not significant, effects on cell viability (Fig. S4a-d; $P > 0.05$). On the other hand, *WDHD1* knockdown in PTEN null type TNBC cell lines (MDA-MB-468, HCC1395 and HCC1937) showed a significant decrease in cell viability (Fig. S4e-g). Although there was a reduction in cell viability with *WDHD1* knockdown in HCC38 cells, no significant difference was observed (Fig. S4h). In general, consistent with the whole genome siRNA screen, depletion of *WDHD1* selectively inhibited cell viability in PTEN null *vs.* WT TNBC cells with 2 individual siRNA oligos against *WDHD1*, although statistical significance for oligo 1# was not reached ($P = 0.054$) (Fig. 5a).

It is known that 3D cell cultures represent their *in vivo* counterparts better than 2D monolayer cell culture models[23,24]. To further validate the effects of *WDHD1* knockdown in TNBC cells, 3D mammosphere assays with PTEN WT (BT20 and MDA-MB-231) and null type (HCC1395 and HCC1937) TNBC cell lines were performed. Images of spheres were analysed for sphere formation efficiency and sphere volume, and cell viability was determined using Cell-Titer Glo® assays. *WDHD1* depletion in PTEN WT TNBC cell lines

(BT20 and MDA-MB-231) showed minimal effects on sphere formation efficiency, sphere volume and cell viability (Fig. S5). In contrast, a significant decrease in sphere formation efficiency, sphere volume and cell viability with two individual siRNA oligos against *WDHD1* was observed in HCC1395 (Fig. 5b; P <0.05) and HCC1937 (Fig. 5c; P < 0.05), both of which are PTEN null type TNBC cell lines.

These experiments showed that WDHD1 is preferentially required by PTEN inactive TNBC cells for survival, but not for those harbouring WT PTEN.

Essential roles of WDHD1 in cell cycle in PTEN null TNBC cell lines.

In order to understand the functions of WDHD1, 92 TNBC samples from the TCGA were identified (Fig. 1a). The top 10% and bottom 10% of samples were separated into two groups: high and low *WDHD1* expressing samples, respectively, and those genes with P values less than 0.05 were considered as differentially expressed genes (DEGs). A heat-map of 3,796 DEGs in the high *vs.* low *WDHD1* groups (P < 0.05) was shown in Fig. S6a. To investigate whether the significantly up-regulated 2,069 genes in the high *WDHD1* group were enriched in certain cellular functions, ToppGene, (https://toppgene.cchmc.org/), was used. We found that the regulation of cell cycle was enriched in the high *WDHD1* TNBC samples (Fig. S6b).

To validate these findings, *WDHD1* expression was depleted by 2 individual siRNA oligos in TNBC cell lines, followed by cell cycle analysis based on flow cytometry (Fig. S7). Interestingly, depletion of *WDHD1* with 2 individual siRNA oligos significantly reduced the percentage of cells in S phase in PTEN null TNBC cells, including MDA-MB-468 (Fig. S7a) and HCC1395 (Fig. S7b). However, no effects on cell cycle were observed in PTEN WT TNBC cell lines, including BT20 (Fig. S7c) and MDA-MB-231 (Fig. S7d).

These results suggested an important role of WDHD1 in cell cycle regulation in PTEN null TNBC cell lines, consistent with the findings in cell viability assays.

Essential roles of WDHD1 in protein translation in PTEN null TNBC cells.

By performing immunoprecipitation - mass spectrometry (IP-MS) analysis, we identified 64 proteins as WDHD1 binding partners in PTEN null MDA-MB-468 cells. Endogenous WDHD1 was immunoprecipitated along with control IgG as negative controls in MDA-MB-468 cells (Fig. 6a) followed by mass spectrometry analysis. Functional enrichment (ToppGene) of WDHD1 binding partners showed a total of 17 functions identified (Table S3). The top 4 functions are shown in Fig. 6b, with protein translation as the top one (Fig. 6b), which suggests a role of WDHD1 in protein translation in PTEN null TNBC cells.

To verify these findings, *WDHD1* expression was depleted by 2 individual siRNA oligos in MDA-MB-468-TR-PTEN cells followed by puromycin incorporation assay to measure protein synthesis. Puromycin is commonly used to study translation[25,26]. Puromycin incorporation stops translation elongation and subsequently induces the release of puromycylated peptides from the ribosome[27]. Unlike radiolabelled amino acids and non-canonical amino acid analogues, puromycin incorporation is not significantly impacted by the endogenous methionine concentration nor the methionine content of proteins[26]. Puromycin thus incorporates relatively equally into all nascent polypeptides, making it a reliable tool for measuring global protein synthesis.

In this study, we utilised the puromycin incorporation assay, in which cells were treated with 2.5 μM puromycin for 5 min before sample collection. We were able to show a 25-30% reduction in global protein translation upon PTEN re-introduction or *WDHD1* depletion (Fig. 6c, d; $P < 0.05$). As a positive control, PTEN expression was induced in MDA-MB-468-TR-

PTEN cells by addition of DOX, since it is known that PTEN inhibits protein translation through negative regulation of mammalian target of rapamycin (mTOR) (Fig. 6c)[28].

As shown in Fig. 6c and d, depletion of *WDHD1* with 2 individual siRNA oligos significantly inhibited global protein translation in MDA-MB-468 cells, reflected by the reductions in the puromycin labelling intensity (Fig. 6d; $P < 0.05$). The inhibitory effect of *WDHD1* depletion on protein translation were similar to those achieved by re-introducing PTEN in MDA-MB-468 cells (Fig. 6c, d), indicating an important role of WDHD1 in protein translation in PTEN null TNBC cells. Interestingly, the phosphorylation level of mTOR was not affected by WDHD1 status (Fig. 6c), indicating that the impact of WDHD1 on protein translation is independent of mTOR. We further validated several interactions of WDHD1 with the potential binding partners (including RPS6 and eIF3β) identified via the IP-MS analysis (Fig. 6e), highlighting the interactions between WDHD1 and the components of translational machinery.

WDHD1 levels are increased in TNBC compared to normal breast tissues, and associate with tumour size and proliferation.

The clinical importance of WDHD1 in TNBC was evaluated in samples from TNBC patients. From TCGA analysis, *WDHD1* mRNA levels were significantly higher in TNBC than the normal breast samples (Fig. 7a; $P < 0.0001$). In addition, the number of patients with T2 and above in the high *WDHD1* group was significantly larger than the low *WDHD1* group (Fig. 7b; $P = 0.027$).

The association between WDHD1 and clinic-pathological features in TNBC patients was further investigated by immunohistochemistry (IHC) staining of WDHD1 in a TNBC tissue

microarray. We found that tumour grade (P = 0.03) and tumour size (P = 0.016) were significantly correlated with WDHD1 expression (Table 1). Representative images of high and low expression of WDHD1 in TNBC are shown in Fig. 7c. Moreover, a positive correlation between WDHD1 expression levels (reflected by its IHC scores) and Ki67 percentage (a proliferation marker) was observed in TNBC (Fig. 7d; Pearson's correlation r = 0.3714; P = 0.0004), suggesting a role of WDHD1 in regulating cell viability, in consistence with the above *in vitro* findings.

Discussion

As TNBC is difficult to be targeted and is molecularly heterogeneous, further stratification is needed. TNBC has been subdivided into 6 distinct subtypes; basal-like 1 (BL1), basal-like 2 (BL2), immunomodulatory (IM), mesenchymal (M), mesenchymal stem-like (MSL) and luminal androgen receptor (LAR)[9]. Another study re-classified TNBC into 5 stable subtypes: BL1, IM, M, MSL and LAR[29]. PTEN inactivation was observed in the BL1 subtype[29], which was further confirmed in a recent *in silico* analysis, showing exceedingly poor clinical outcome[30].

Loss-of-function mutations in tumour suppressor genes (TSGs), such as *PTEN*, are major genetic alterations leading to more challenges to identify targeted drugs since it is difficult to restore their functions[31]. Therefore, studies have been focused to target downstream signalling pathways that are altered by inactivation of TSGs[18,31]. Targeting synthetic lethality provides an alternative approach[32]. As the second most mutated gene following p53 in various cancer types[33], various studies have been performed to identify *PTEN* synthetic lethal interactions in a variety of cancer types. These include mitochondrial complex I inhibitors[34] and chromatin helicase DNA-binding factor *CHD1* in PTEN-inactive prostate cancer cells[35], polynucleotide kinase/phosphatase (*PNKP*) in PTEN-deficient lung and colon cancer cells, and NUAK family kinase 1 (*NUAK1*) in PTEN-deficient breast cancer cells[36]. In this study, using TCGA analysis coupled with a whole genome siRNA screen in isogenic PTEN negative and positive TNBC cells, we identified *WDHD1* as a synthetic essential gene in PTEN-inactive TNBC cells.

WDHD1, an orthologue of *Ctf4* in budding yeast[37] and *Mcl1* in fission yeast[38], is a DNA binding protein[39] that is known to play important roles in DNA replication and cell cycle[37,40–46]. We also observed an important role of WDHD1 in cell cycle, especially in PTEN-inactive

TNBC cells. The selective killing of *WDHD1* depletion in PTEN-inactive TNBC cells was further validated in both 2D and 3D cultures. In addition, using IP-MS analysis followed by bioinformatics, we identified a potential, yet unknown function of WDHD1 in protein translation in PTEN null TNBC cells, which was further validated with puromycin incorporation assay to measure global protein synthesis. Depletion of *WDHD1* significantly inhibits global protein translation in PTEN null TNBC cells, which is independent of mTOR inhibition and potentially via directly interacting with the translational machinery. The impact of WDHD1 depletion on global protein translation is similar to the effect achieved by re-introducing PTEN. PTEN inactivation in TNBC leads to a high activity of mTOR[47], which is linked to a high rate of protein synthesis, creating an "Achilles heel" of TNBC. Indeed, several clinical trials on Everolimus (a mTOR inhibitor) in TNBC are ongoing (clinicaltrials.gov), some of which showed positive results[48,49]. However, a common pattern seen in trial data is of a modest response to rapalog (rapamycin and its analogs) monotherapy, which does not lead to a significant improvement in patient outcomes. One of the likely reasons is that it is caused by reactivation of signalling pathways that drive the high rate of protein synthesis required by tumour growth. Inhibition of WDHD1 in a PTEN inactive background reduces protein translation, suggesting that such a "synthetic sickness" approach may be applicable to PTEN-deficient tumours when rapalog resistance happens.

In addition, a potential role of WDHD1 in regulating the stemness of PTEN inactive TNBC cells was investigated using a mammosphere formation assay, which is one of the assays used to determine cell stemness[50]. Given the impact of WDHD1 on cell cycle and protein translation, both of which play important roles in regulating cell stemness[51], we presume that WDHD1 may control stemness in PTEN inactive TNBC cells via its ability to regulate cell cycle and protein translation, however, this remains to be elucidated. We found WDHD1 expression is significantly higher in PTEN-inactive TNBC cells than in PTEN-

active ones. A previous report from Sato and colleagues suggested that AKT kinase seems to phosphorylate and stabilise the WDHD1 protein in cancer cells[44]. In addition to the reported effects of AKT on WDHD1 protein stability, we found the mRNA levels of *WDHD1* are also regulated by the PTEN-AKT pathway. Together, this data suggests that WDHD1 expression is affected by PTEN-AKT signalling in TNBC cells at both mRNA and protein levels.

The clinical importance of WDHD1 in TNBC was evaluated in samples obtained from TNBC patients, showing that its levels are increased in TNBC compared to normal breast tissues, and associates with tumour size, stage and proliferation, using Ki67 as a proliferation marker[52]. Moreover, recent reports demonstrated that overexpression of WDHD1 leads to cisplatin resistance in lung adenocarcinoma[53] and metastasis in cholangiocarcinoma[54]. Further studies are required to confirm these findings in TNBC. The data presented here suggests that inhibitors that can disrupt the interactions between WDHD1 and the protein synthesis machinery could target some of the most intractable tumour types, such as TNBC with PTEN-deficiency. The relatively mild effects of *WDHD1* depletion in PTEN positive cells suggests that on-target inhibition of this factor may also be relatively free from unwanted side effects.

Materials and Methods

Cell culture, transfections and reagents

Human breast cancer cell lines (HCC1806, BT20, MDA-MB-157, MDA-MB-231, MDA-MB-468, HCC1395, HCC1937 and HCC38) were obtained as NCI-ICBP45 kit procured through American Type Culture Collection (ATCC) (ATCC Breast Cancer Cell Panel, Manassas, VA, USA). Cell lines were authenticated by ATCC using short tandem repeat DNA profiling, and each cell culture was examined by light microscopy and compared with images published by ATCC and the Integrative Cancer Biology Program (ICBP; http://icbp.lbl.gov/breastcancer/celllines.php) to verify identity[55]. HCC1806, HCC1395, HCC1937 and HCC38 cells were maintained in Roswell Park Memorial Institute (RPMI) 1640 medium, (Gibco® by life technology) with 10% FBS and 1% (v/v) Penicillin/Streptomycin, (Gibco® by life technology). BT20, MDA-MB-157, MDA-MB-231, MDA-MB-468 and MDA-MB-468-TR-PTEN cell lines were maintained in Dulbecco's Modified Eagle's Medium (DMEM), (Gibco® by life technology) with 10% FBS and 1% (v/v) Penicillin/Streptomycin. All cells were kept at 37°C and 5% CO_2. No mycoplasma contamination was detected in the cell lines used. AKT VIII and puromycin were from Sigma Aldrich.

For PTEN-inducible cells, MDA-MB-468 cells were stably transfected with a tetracycline-inducible PTEN vector and named MDA-MB-468-TR-PTEN, in which addition of Doxycycline (DOX) acutely induces PTEN expression. MDA-MB-468 cells were also stably transfected with a tetracycline-inducible parent vector and used as vector-only controls (MDA-MB-468-TR-EV). To fluorescently label MDA-MB-468-TR-PTEN and MDA-MB-468-TR-EV cells, pCherryFP-N1 and p-EGFP-N1 were stably transfected into them,

respectively. Single clones were picked and sorted by fluorescence-activated cell sorting (FACS), and named as MDA-MB-468-TR-PTEN/CherryFP or MDA-MB-468-TR-EV/GFP.

Short interfering RNA (siRNA) oligos against WDHD1 *(D-019780-02* and *D-019780-03)* was purchased from Dharmacon. Sequences are available from Dharmacon, or upon request. siGENOME RISC-Free siRNA (Dharmacon) was used as a negative control. Cells were transfected with the indicated siRNA oligos at a final concentration of 35 nM using Dharmafect 2 reagent (Dharmacon).

The Cancer Genome Atlas (TCGA) data analysis

Expression of genes/proteins of interest, obtained from the cBioPortal for Cancer Genomics (https://www.cbioportal.org/) and UCSC Cancer Genome Browser (https://genome-cancer.ucsc.edu/), were analysed in each breast cancer molecular subtype along with normal breast samples (details provided in Supplementary Methods).

A whole genome siRNA screen and data analysis

The human siGENOME siRNA library - Genome (G-005005) was obtained from Dharmacon. siRNA transfection experiments were performed in 96-well format in antibiotic-free medium, using a reverse transfection employing 25 nM siRNA and 0.15 µl Dharmafect 2 (Dharmacon) per well together with a starting cell density optimized to produce an 80% confluent monolayer in mock-treated cells at the conclusion of the experiment. DOX-treated MDA-MB-468-TR-PTEN/CherryFP (PTEN+) or MDA-MB-468-TR-EV/GFP (PTEN-) cells were mixed and transfected at a 1:1 ratio in 96-well plates. Cells were fixed with 4%

paraformaldehyde at 96 h post transfection. Fluorescence was read on an EnVision 2102 Plate-reader (Perkin-Elmer).

Triplicate data points from CherryFP channel (PTEN+) and GFP channel (PTEN-) screens underwent plate and position normalization and Z-score calculation using cellHTS software[56,57]. Differential Z-scores (Δ Z-score) between the two channels were subsequently used to create a gene hit list. Reproducibility of the replicates was analysed by performing Pearson correlation analysis in GraphPad Prism 8. *P*-value < 0.05 was considered significant (details provided in Supplementary Methods).

Cell viability assay

siRNA transfected cells were plated into 96-well plate with a density of 8,000 cells/well. CellTiter-Glo® Luminescent cell viability assay (Promega) was performed 96 hours post transfection according to the manufacturer's protocol using GloMax® Discover Microplate Reader (Promega).

Mammosphere assay and quantifications

siRNA transfections were performed in 2D cultures. 96 hours post-transfections, cells were cultured in 96-well ultralow attachment plate in 100 µl at plating densities between 3,000 and 7,000 cells/well. Cells were cultured in 1:1 DMEM:F12, (Gibco® by life technology) media plus 1% P/S, 2% B27, (Gibco® by life technology), 20 ng/ml EGF, (PEPROTECH) and 20 ng/ml bFGF, (PEPROTECH) at 37°C and 5% CO_2 for 14 days. After the incubation period, the images were taken using with 40X magnification.

The mammospheres that were equal to or greater than 50 micrometres in diameter were counted to calculate the mammosphere formation efficiency (MFE%) with the following equation: (# of mammospheres per well) / (# of cells seeded per well) x 100. Additionally, the volumes of the mammospheres were also calculated using the formula of Volume = $(4/3)\pi r^3$. ImageJ (version1.42q) was used to determine the MFE and volume of sphere.

CellTiter-Glo® cell viability assay was performed with addition of 100 µl of CellTiter-Glo® reagent into each well and incubated at room temperature for 1 hour, followed by measuring using GloMax® Discover Microplate Reader (Promega).

Western blot analysis

Western blot analysis was performed with lysates from cells lysed with urea buffer (8M urea, 1M thiourea, 0.5% CHAPS, 50 mM DTT and 24 mM spermine). The bound proteins were separated on SDS polyacrylamide gels and subjected to immunoblotting with the indicated antibodies. For immunoprecipitations, the cells were lysed for 30 min at 4 °C in pNAS buffer [50 mm Tris/HCl (pH 7.5), 120 mm NaCl, 1 mm EDTA and 0.1% Nonidet P-40], with protease inhibitors. Anti-WDHD1 (Sigma-Aldrich) or control antibodies and Protein G magnetic beads (Thermo Fisher Scientific) were added to the lysate for 16 h at 4 °C. Immunoprecipitates were washed four times with cold PBS followed by the addition of SDS sample buffer. The bound proteins were separated on SDS polyacrylamide gels and subjected to immunoblotting with the indicated antibodies. Primary antibodies were from Cell Signalling Technology (PTEN (D4.3) XP®, 1:1000, 9188; phospho-AKT (Thr308) (244F9), 1:1000, 4056; phospho-AKT (Ser473), 1:1000, 9271; AKT, 1:1000, 9272; Phospho-ERK, 1:1000, 9101; ERK, 1:1000, 9102; Phospho-mTOR (Ser2448), 1:1000, 2971; β-tubulin (D3U1W), 1:1000, 86298), Sigma-Aldrich (WDHD1, 1:500, HPA001122; Puromycin,

1:2000, MABE343), PROTEINTECH (GAPDH, 1:10000, 10494-1-AP), Santa Cruz Biotechnology (RPS6 (C-8), 1:500, sc-74459; eIF3β (A7), 1:500, sc-374156). Signals were detected using an Odyssey imaging system (LI-COR) or an ECL detection system (GE Healthcare, Chicago, IL, USA), and evaluated by ImageJ (version1.42q) software (National Institutes of Health) (Berhesda, MD, USA).

qRT-PCR

RNA extraction was performed by RNeasy® Mini Kit (Qiagen) manufacturer's protocol and Nanodrop Spectrophometer 2000c (Thermo Fisher Scientific) was used to quantify RNA concentration. QuantiNova™ SYBR Green RT-PCR kits (Qiagen) were used with *WDHD1* (QT00062244) and *ACTB* (β-actin, QT00095431) gene-specific primers (QuantiTect Primer Assays, Qiagen). Relative mRNA levels of target genes were normalised to *ACTB* (β-actin).

Immunofluorescence microscopy

Cells were fixed in 4% PBS-paraformaldehyde for 15 minutes, incubated in 0.1% Triton-X-100 for 5 minutes on ice, then in 0.2% Fish Skin Gelatine in PBS for 1 hour and stained for 1 hour with an anti-WDHD1 (1:500, Sigma-Aldrich, HPA001122). Protein expression was detected using Alexa Fluor (1:400, Molecular Probes) for 20 minutes. DAPI (Invitrogen) was used to stain nuclei (1:1000). Samples were observed using a confocal microscope system (Leica SP8). Acquired images were analysed using Fiji[58].

Immunohistochemical and H/E staining and scoring

Tissue microarray of TNBC patients with information of clinic-pathological parameters was purchased from Outdo Biotech (HBreD090Bc01; Shanghai, China). Tissue samples were pre-stained with Ki67. All procedures were approved by the Ethical Committee of Tongji Hospital, China. Informed consent was obtained from all subjects. For immunohistochemical staining, antigen retrieval, blocking of non-specific binding and incubation of primary antibodies at 4°C overnight were conducted sequentially. The primary antibody of anti-WDHD1 (HPA001122, Sigma-Aldrich, 1:500) was used. After incubation with secondary goat anti-rabbit immunoglobulin conjugated to peroxidase-labelled dextran polymer (SV0002; Boster) at 37°C for 1 h, visualization, counterstaining with haematoxylin and mounting were performed. Semi-quantitative evaluations of protein expression were scored on the basis of the intensity and the percentage of WDHD1 positive tumour cells as previously described[59–62].

Flow cytometry

For cell cycle analysis, 48 hours post transfection, cells were fixed with 70% ethanol and kept at 4°C for up to 2 weeks. Cells were treated with 0.25% Triton-X-100, 200 μg/ml RNAse A and 50 μg/ml propidium iodide (PI), and analysed by fluorescence-activated cell sorting (FACS), Guava.

Immunoprecipitation - mass spectrometry (IP-MS) analysis

For immunoprecipitations of endogenous WDHD1, the cells were lysed for 30 min at 4 °C in pNAS buffer [50 mm Tris/HCl (pH 7.5), 120 mm NaCl, 1 mm EDTA and 0.1% Nonidet P-40], with protease inhibitors. Anti-WDHD1 (Sigma-Aldrich) or control antibodies and

Protein G Sepharose (GE Healthcare) were added to the lysate for 16 h at 4 °C. Immunoprecipitates were washed four times with cold PBS followed by mass spectrometry analysis (details provided in Supplementary Methods).

Two repeats of WDHD1 and two repeats of IgG control samples were combined in RStudio (version 3.4.4), and the proteins with *NA* values in more than 2 samples were removed. The average of peptide numbers for WDHD1 and IgG control samples was calculated and ratio of peptide numbers for each sample group was calculated. The proteins which had 2 times higher peptide number in WDHD1 compared to the control samples were chosen as threshold and used to perform pathway analysis in ToppGene website as described below.

Bioinformatics

For pathway analysis, ToppGene Suite (https://toppgene.cchmc.org/) was used to detect functional enrichment of the mRNAs or proteins. The pathways were sorted from lowest *P*-value and top 15 pathways were chosen for TCGA data. We then produced a histogram plot with the top 15 pathways in GraphPad Prism 8. The pathways for IP-MS data were sorted from lowest *P*-value and the histogram was plotted with top 4 pathways in GraphPad Prism 8.

Statistical analysis

Two tailed, unpaired Student's *t-test* for the TCGA data and two paired, paired Student's *t-test* for the whole genome siRNA screening data were performed in RStudio (version 3.4.4). Codes are available upon request. Unless stated otherwise, comparison of two groups was statistically calculated by two paired, unpaired Student's *t*-test in GraphPad Prism 8 software.

Ordinary one-way ANOVA was conducted to statistically compare more than two groups in GraphPad Prism 8 software. Correlation analysis was conducted by Pearson's correlation in GraphPad Prism 8 software. $\chi 2$ test was used to analyse the association of PTEN and WDHD1 with clinical features of TNBC samples in the TCGA breast invasive carcinoma data in GraphPad Prism 8 software. $\chi 2$ test or Fisher's exact test was used to evaluate the relationship of WDHD1 and clinic-pathological parameters of TNBC patient samples in IHC using SPSS (version 19.0). Data were shown as box and whisker plot with minimum and maximum individual values, mean ± SD or mean ± SEM, indicated in figure legend.

Acknowledgements

This project was supported by an Academy of Medical Sciences/the Wellcome Trust Springboard Award [SBF002\1038], Medical Research Council [MR/S025480/1] and the National Natural Science Foundation of China [81772827]. AE was supported by the Wessex Medical Trust. CH was supported by Gerald Kerkut Charitable Trust and University of Southampton Central VC Scholarship Scheme. MRP was supported by the Wellcome Trust [208908/Z/17/Z]. PS was supported by Against Breast Cancer. JD was supported by the Francis Crick Institute which receives its core funding from Cancer Research UK (FC001070), the UK Medical Research Council (FC001070) and the Wellcome Trust (FC001070). Instrumentation in the Centre for Proteomic Research is supported by the BBSRC [BM/M012387/1] and the Wessex Medical Trust. We thank Dr. Noor Shamkhi for her technical help in flow cytometry, Fuad M. M. Alzahrani for the puromycin incorporation assay and Matt Sherwood for the 3D mammosphere assay.

Conflict of interest

The authors declare that they have no conflict of interest.

References

1. Bray, F. *et al.* Global cancer statistics 2018: GLOBOCAN estimates of incidence and mortality worldwide for 36 cancers in 185 countries. *CA. Cancer J. Clin.* **68**, 394–424 (2018).

2. O'Reilly, E. A. *et al.* The fate of chemoresistance in triple negative breast cancer (TNBC). *BBA Clin.* **3**, 257–275 (2015).

3. Reis-Filho, J. S. & Tutt, A. N. J. Triple negative tumours: A critical review. *Histopathology* **52**, 108–118 (2008).

4. Carey, L. A. *et al.* Race, Breast Cancer Subtypes, and Survival in the Carolina Breast Cancer Study. *JAMA* **295**, 2492–2502 (2006).

5. Kulkarni, A. *et al.* Breast Cancer Incidence and Mortality by Molecular Subtype: Statewide Age and Racial/Ethnic Disparities in New Jersey. *Cancer Heal. disparities* **3**, e1–e17 (2019).

6. Lee, A. & Djamgoz, M. B. A. Triple negative breast cancer: Emerging therapeutic modalities and novel combination therapies. *Cancer Treat. Rev.* **62**, 110–122 (2018).

7. Khosravi-Shahi, P., Cabezón-Gutiérrez, L. & Custodio-Cabello, S. Metastatic triple negative breast cancer: Optimizing treatment options, new and emerging targeted therapies. *Asia. Pac. J. Clin. Oncol.* **14**, 32–39 (2018).

8. Cyprian, F. S., Akhtar, S., Gatalica, Z. & Vranic, S. Targeted immunotherapy with a checkpoint inhibitor in combination with chemotherapy: A new clinical paradigm in the treatment of triple-negative breast cancer. *Bosn. J. Basic Med. Sci.* **19**, 227–233 (2019).

9. Lehmann, B. D. *et al.* Identification of human triple-negative breast cancer subtypes and preclinical models for selection of targeted therapies. *J. Clin. Invest.* **121**, 2750–2767 (2011).

10. López-Knowles, E. *et al.* PI3K pathway activation in breast cancer is associated with the basal-like phenotype and cancer-specific mortality. *Int. J. Cancer* **126**, 1121–1131 (2010).

11. Beg, S. *et al.* Loss of PTEN expression is associated with aggressive behavior and poor prognosis in Middle Eastern triple-negative breast cancer. *Breast Cancer Res. Treat.* **151**, 541–553 (2015).

12. Li, S. *et al.* Loss of PTEN expression in breast cancer: association with clinicopathological characteristics and prognosis. *Oncotarget* **8**, 32043–32054 (2017).

13. Song, M. S., Salmena, L. & Pandolfi, P. P. The functions and regulation of the PTEN tumour suppressor. *Nat. Rev. Mol. Cell Biol.* **13**, 283–296 (2012).

14. Myers, M. P. *et al.* P-TEN, the tumor suppressor from human chromosome 10q23, is a dual-specificity phosphatase. *Proc. Natl. Acad. Sci.* **94**, 9052–9057 (1997).

15. Georgescu, M. M., Kirsch, K. H., Akagi, T., Shishido, T. & Hanafusa, H. The tumor-suppressor activity of PTEN is regulated by its carboxyl-terminal region. *Proc. Natl. Acad. Sci. U. S. A.* **96**, 10182–10187 (1999).

16. Fanning, A. S. & Anderson, J. M. Protein modules as organizers of membrane structure. *Curr. Opin. Cell Biol.* **11**, 432–439 (1999).

17. Fece de la Cruz, F., Gapp, B. V. & Nijman, S. M. B. Synthetic lethal vulnerabilities of cancer. *Annu. Rev. Pharmacol. Toxicol.* **55**, 513–531 (2014).

18. Brunen, D. & Bernards, R. Drug therapy: Exploiting synthetic lethality to improve cancer therapy. *Nat. Rev. Clin. Oncol.* **14**, 331–332 (2017).

19. Brummelkamp, T. R. & Bernards, R. New tools for functional mammalian cancer genetics. *Nat. Rev. Cancer* **3**, 781–789 (2003).

20. Farmer, H. *et al.* Targeting the DNA repair defect in BRCA mutant cells as a therapeutic strategy. *Nature* **434**, 917–921 (2005).

21. Bryant, H. E. *et al.* Specific killing of BRCA2-deficient tumours with inhibitors of poly(ADP-ribose) polymerase. *Nature* **434**, 913–917 (2005).

22. Carnero, A. The PKB/AKT pathway in cancer. *Curr. Pharm. Des.* **16**, 34–44 (2010).

23. Pampaloni, F., Reynaud, E. G. & Stelzer, E. H. K. The third dimension bridges the gap between cell culture and live tissue. *Nat. Rev. Mol. Cell Biol.* **8**, 839–845 (2007).

24. Yamada, K. M. & Cukierman, E. Modeling Tissue Morphogenesis and Cancer in 3D. *Cell* **130**, 601–610 (2007).

25. Dermit, M., Dodel, M. & Mardakheh, F. K. Methods for monitoring and measurement of protein translation in time and space. *Mol. Biosyst.* **13**, 2477–2488 (2017).

26. Hidalgo, L., Jose, S. & Signer, R. A. J. Cell-type-speci fi c quanti fi cation of protein synthesis in vivo. *Nat. protcols* **14**, 441–460 (2019).

27. Nathans, D. Inhibition of Protein Synthesis By Puromycin. *Proc. Natl. Acad. Sci. U. S. A.* **51**, 585–592 (1964).

28. Simpson, L. & Parsons, R. PTEN: Life as a tumor suppressor. *Exp. Cell Res.* **264**, 29–41 (2001).

29. Bareche, Y. *et al.* Unravelling triple-negative breast cancer molecular heterogeneity using an integrative multiomic analysis. *Ann. Oncol.* **29**, 895–902 (2018).

30. Wang, D. Y., Jiang, Z., Ben-David, Y., Woodgett, J. R. & Zacksenhaus, E. Molecular stratification within triple-negative breast cancer subtypes. *Sci. Rep.* **9**, 19107 (2019).

31. Hartwell, L. H., Szankasi, P., Roberts, C. J., Murray, A. W. & Friend, S. H. Integrating genetic approaches into the discovery of anticancer drugs. *Science (80-.).* **278**, 1064–1068 (1997).

32. Doye, V. & Hurt, E. C. Genetic approaches to nuclear pore structure and function. *Trends Genet.* **11**, 235–241 (1995).

33. Kechagioglou, P. *et al.* Tumor suppressor PTEN in breast cancer: Heterozygosity, mutations and protein expression. *Anticancer Res.* **34**, 1387–1400 (2014).

34. Naguib, A. *et al.* Mitochondrial complex I inhibitors expose a vulnerability for selective killing of Pten-null cells. *Cell Rep.* **23**, 58–67 (2018).

35. Zhao, D. *et al.* Synthetic essentiality of chromatin remodelling factor CHD1 in PTEN-

deficient cancer. *Nature* **542**, 484–488 (2017).

36. Tang, Y. C. *et al.* Functional genomics identifies specific vulnerabilities in PTEN-deficient breast cancer. *Breast Cancer Res.* **20**, 22 (2018).

37. Kang, Y.-H. *et al.* Interaction between human Ctf4 and the Cdc45/Mcm2-7/GINS (CMG) replicative helicase. *Proc. Natl. Acad. Sci.* **110**, 19760–19765 (2013).

38. Williams, D. R. & Mcintosh, J. R. mcl1+, the Schizosaccharomyces pombe homologue of CTF4, is important for chromosome replication, cohesion, and segregation. *Eukaryot. Cell* **1**, 758–773 (2002).

39. Koehler, A., Schmidt-Zachmann, M. S. & Franke, W. W. AND-1, a natural chimeric DNA-binding protein, combines an HMG-box with regulatory WD-repeats. *J. Cell Sci.* **110**, 1051–1062 (1997).

40. Kilkenny, M. L. *et al.* The human CTF4-orthologue AND-1 interacts with DNA polymerase a/primase via its unique C-Terminal HMG box. *Open Biol.* **7**, 170217 (2017).

41. Abe, T. *et al.* AND-1 fork protection function prevents fork resection and is essential for proliferation. *Nat. Commun.* **9**, 3091 (2018).

42. Bermudez, V. P., Farina, A., Tappin, I. & Hurwitz, J. Influence of the human cohesion establishment factor Ctf4/AND-1 on DNA replication. *J. Biol. Chem.* **285**, 9493–9505 (2010).

43. Zhu, W. *et al.* Mcm10 and And-1/CTF4 recruit DNA polymerase α to chromatin for initiation of DNA replication. *Genes Dev.* **21**, 2288–2299 (2007).

44. Sato, N. *et al.* Activation of WD Repeat and High-Mobility Group Box DNA Binding Protein 1 in Pulmonary and Esophageal Carcinogenesis. *Clin. Cancer Res.* **16**, 226–239 (2009).

45. Zhou, Y. *et al.* Role of WDHD1 in Human Papillomavirus-Mediated Oncogenesis Identified by Transcriptional Profiling of E7-Expressing Cells. *J. Virol.* **90**, 6071–6084 (2016).

46. Guan, C., Li, J., Sun, D., Liu, Y. & Liang, H. The structure and polymerase-recognition mechanism of the crucial adaptor protein AND-1 in the human replisome. *J. Biol. Chem.* **292**, 9627–9636 (2017).

47. Ní Bhaoighill, M. & Dunlop, E. A. Mechanistic target of rapamycin inhibitors: successes and challenges as cancer therapeutics. *Cancer Drug Resist.* **2**, 1069–1085 (2019).

48. Lee, J. S. *et al.* Phase I clinical trial of the combination of eribulin and everolimus in patients with metastatic triple-negative breast cancer. *Breast Cancer Res.* **21**, 119 (2019).

49. Singh, J. C. *et al.* Phase 2 trial of everolimus and carboplatin combination in patients with triple negative metastatic breast cancer. *Breast Cancer Res.* **16**, R32 (2014).

50. Nalla, L. V., Kalia, K. & Khairnar, A. Self-renewal signaling pathways in breast cancer stem cells. *Int. J. Biochem. Cell Biol.* **107**, 140–153 (2019).

51. Tahmasebi, S., Amiri, M. & Sonenberg, N. Translational control in stem cells. *Front.*

Genet. **9**, 709 (2019).

52. Sahebjam, S. *et al.* Ki 67 is a major, but not the sole determinant of Oncotype Dx recurrence score. *Br. J. Cancer* **105**, 1342–1345 (2011).

53. Gong, L. *et al.* WDHD1 leads to cisplatin resistance by promoting MAPRE2 ubiquitination in lung adenocarcinoma. *Front. Oncol.* **10**, 461 (2020).

54. Liu, B., Hu, Y., Qin, L., Peng, X. Bin & Huang, Y. X. MicroRNA-494-dependent WDHDI inhibition suppresses epithelial-mesenchymal transition, tumor growth and metastasis in cholangiocarcinoma. *Dig. Liver Dis.* **51**, 397–411 (2018).

55. Weigelt, B., Warne, P. H. & Downward, J. PIK3CA mutation, but not PTEN loss of function, determines the sensitivity of breast cancer cells to mTOR inhibitory drugs. *Oncogene* **30**, 3222–3233 (2011).

56. Boutros, M., Brás, L. P. & Huber, W. Analysis of cell-based RNAi screens. *Genome Biol.* **7**, R66 (2006).

57. Steckel, M. *et al.* Determination of synthetic lethal interactions in KRAS oncogene-dependent cancer cells reveals novel therapeutic targeting strategies. *Cell Res.* **22**, 1227–1245 (2012).

58. Schindelin, J. *et al.* Fiji - an Open platform for biological image analysis. *Nat. Methods* **9**, 676–782 (2012).

59. Wang, Y. *et al.* ASPP2 controls epithelial plasticity and inhibits metastasis through β 2-catenin-dependent regulation of ZEB1. *Nat. Cell Biol.* **16**, 1092–1104 (2014).

60. Wang, Y. *et al.* Autophagy inhibition specifically promotes epithelial-mesenchymal transition and invasion in RAS-mutated cancer cells. *Autophagy* **15**, 886–899 (2019).

61. Liu, H. *et al.* SGLT1 is required for the survival of triple-negative breast cancer cells via potentiation of EGFR activity. *Mol. Oncol.* **13**, 1874–1886 (2019).

62. Liu, D. *et al.* ASPP1 deficiency promotes epithelial-mesenchymal transition, invasion and metastasis in colorectal cancer. *Cell Death Dis.* **11**, 224 (2020).

Table

Table 1 The relationship between patients' clinical–pathological characteristics and WDHD1 expression in TNBC.

Characteristics	N	WDHD1		*P* value
		Low expression	High expression	
Age	90			
≤ 50	46	26	20	
＞50	44	23	21	0.686
Location	90			
Left breast	46	25	21	
Right breast	44	24	20	0.985
Grade	90			
I-II	36	25	11	
III	54	24	30	***0.030***
Size	86			
≤ 2cm	37	26	11	
＞2cm	49	21	28	***0.016***
Positive LN	35			
≤ 2	21	9	12	1.000
＞2	14	6	8	

P values were calculated by $\chi 2$ test or Fisher's exact test, if appropriate. LN: lymph node.

Figure Legends

Fig. 1 Candidate genes essential for the survival of PTEN-inactive TNBC cells are identified by the TCGA analysis and a whole genome siRNA screen.

a Workflow showing the analysis to identify 47 candidate genes essential for the survival of PTEN-inactive TNBC cells. **b** Heat-map showing 47 candidate mRNAs that are over-expressed in TNBC samples with the low PTEN compared to those with the high PTEN from TCGA analysis. Red indicates up-regulation and blue for down-regulation. $n = 10$ per group. **c** Heat-map showing 47 candidate genes that are required for the survival of PTEN negative TNBC cells from a whole genome siRNA screen. Red indicates high Z-scores and blue for low Z-scores. $n = 3$ per group.

Fig. 2 WDHD1 is highly expressed in PTEN-inactive TNBC cells.

a Protein expression of WDHD1 and PTEN in the indicated TNBC cell lines with PTEN WT (wild-type) or PTEN null. β-tubulin was used as a loading control. **b** Graph showing protein levels of WDHD1 in PTEN WT or PTEN null TNBC cell lines. $*P < 0.05$. **c** Fold change in mRNA levels of *WDHD1* in the indicated PTEN WT or PTEN null TNBC cell lines. *WDHD1* mRNA expression was normalised to a housekeeping gene, β-actin. Data are mean ± SEM. $n = 3$. **d** Graph showing mRNA levels of *WDHD1* in PTEN WT or PTEN null TNBC cell lines. $**P < 0.01$. Data in (**b**) and (**d**) are individual values with mean, and error bars indicate minimum and maximum individual values. $n = 4$ per group.

Fig. 3 WDHD1 levels are reduced upon PTEN expression in MDA-MB-468 cells.

a Protein expression of PTEN and WDHD1 in MDA-MB-468-TR-PTEN cells treated with or without doxycycline (DOX). β-tubulin was used as a loading control. Adding DOX induces PTEN expression in MDA-MB-468-TR-PTEN cells. Graphs showing protein (**b**) or mRNA (**c**) levels of WDHD1 in MDA-MB-468-TR-PTEN cells treated with (DOX+) or without DOX (DOX-). $^{**}P < 0.01$. $^{****}P < 0.0001$. Data are mean ± SEM. $n = 3$ per group. **d** Immunofluorescence staining of WDHD1 (green) in MDA-MB-468-TR-PTEN cells treated with (DOX+) or without DOX (DOX-). DAPI (blue) was used to stain nuclei. Scale bars: 20 μm.

Fig. 4 WDHD1 levels are reduced upon AKT inhibition in PTEN null TNBC cells.

Protein expression of WDHD1, phospho-AKT (pAKT) (Thr308) and pAKT (Ser473) in MDA-MB-468 (**a**), HCC1395 (**b**), HCC1937 (**c**) and HCC38 (**d**) treated with DMSO or an AKT inhibitor, AKT VIII (10 μM). β-tubulin was used as a loading control. Graphs showing protein levels of WDHD1 in MDA-MB-468 (**a**), HCC1395 (**b**), HCC1937 (**c**) and HCC38 (**d**) treated with DMSO or AKT VIII. $^{*}P < 0.05$. Data are mean ± SEM. $n = 3$ per group. **e** The scatter plot for the correlation between pAKT_308, protein expression (RPPA) and *WDHD1*, mRNA expression (IlluminaHiSeq) in the TCGA breast invasive carcinoma (Provisional) data (Pearson's correlation (r) = 0.3321; $P = 0.0296$; $n = 43$).

Fig. 5 WDHD1 is required for the survival of PTEN null TNBC cells cultured in 2D or 3D.

a Graph showing relative cell viability in PTEN WT or PTEN null TNBC cell lines transfected with control or *WDHD1* siRNAs in 2D cultures. Cell-Titer Glo® assay was performed to measure cell viability. Representative phase contrast microscopy images of PTEN null type TNBC cell line HCC1395 (**b**) or HCC1937 (**c**) with indicated transfections cultured in 3D. Scale bar: 50 μm. Graphs showing sphere formation efficiency, sphere volume and cell viability (Cell-Titer Glo® assay) in HCC1395 (**b**) or HCC1937 (**c**) with indicated transfections cultured in 3D. Data are mean ± SEM. $n = 3$ samples per group. *$P <$ 0.05. **$P < 0.01$. ***$P < 0.001$. ****$P < 0.0001$.

Fig. 6 Essential roles of WDHD1 in protein translation in PTEN null TNBC cells.

a Total cell lysates from MDA-MB-468 cell were immunoprecipitated with an anti-WDHD1 antibody or control IgG. WDHD1, IgG heavy and light chains are indicated. **b** Functional enrichment (ToppGene) of WDHD1 binding partners identified from an immunoprecipitation - mass spectrometry (IP-MS) experiment is visualised on a bar chart, showing number of shared proteins and -Log10 (*P* value). *P* values less than 0.0001 are shown. **c** Puromycin labelling to measure protein synthesis in MDA-MB-468-TR-PTEN cells with indicated treatments. Equal amounts of total protein extracts were analysed by western blotting showing levels of PTEN, WDHD1, phospho-mTOR (p-mTOR) and puromycin labelling. GAPDH was used as a loading control. Ponceau S staining showing total protein levels. **d** Graph showing relative puromycin labelling intensity in MDA-MB-468-TR-PTEN cells with indicated treatments. Data are mean ± SEM. $n = 4$ samples per group. * $P < 0.05$. ** $P < 0.01$. ns: not significant, $P > 0.05$. **e** Total cell lysates from MDA-MB-468 cell were

immunoprecipitated with an anti-WDHD1 antibody or control IgG. RPS6, eIF3β and WDHD1 are indicated.

Fig. 7 WDHD1 levels are increased in TNBC compared to normal breast tissues, and associates with tumour size and proliferation.

a Graph showing *WDHD1*, mRNA levels (Z-scores) in the normal breast (n = 36) and TNBC (n = 171) samples obtained from the TCGA data. Data are mean ± SD. ****P < 0.0001. **b** Graph showing the number of TNBC patients (TCGA) with T2 and above or < T2 in the low or high *WDHD1* group. *P < 0.05. **c** Representative WDHD1 staining pattern (high or low WDHD1) in TNBC tissue microarray cores. Scale bar: 100 μm. **d** The scatter plot for the correlation between WDHD1 scores and percentage of Ki67-positive cells in TNBC samples (Pearson's correlation r = 0.3714; P = 0.0004; n = 88).

Figure 1

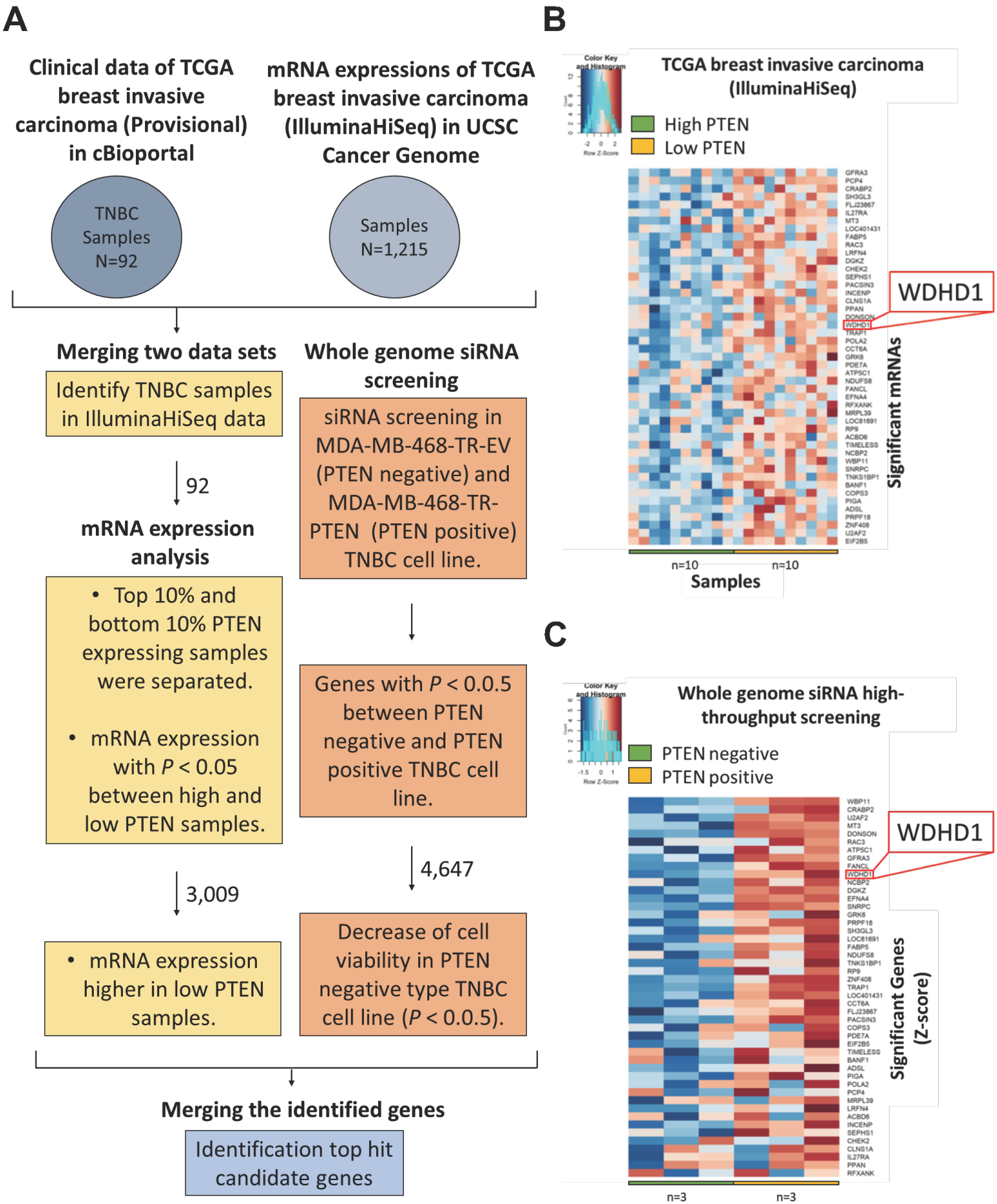
A
Clinical data of TCGA breast invasive carcinoma (Provisional) in cBioportal
mRNA expressions of TCGA breast invasive carcinoma (IlluminaHiSeq) in UCSC Cancer Genome
TNBC Samples N=92
Samples N=1,215
Merging two data sets
Identify TNBC samples in IlluminaHiSeq data
92
mRNA expression analysis
• Top 10% and bottom 10% PTEN expressing samples were separated.
• mRNA expression with P < 0.05 between high and low PTEN samples.
3,009
• mRNA expression higher in low PTEN samples.
Whole genome siRNA screening
siRNA screening in MDA-MB-468-TR-EV (PTEN negative) and MDA-MB-468-TR-PTEN (PTEN positive) TNBC cell line.
Genes with P < 0.0.5 between PTEN negative and PTEN positive TNBC cell line.
4,647
Decrease of cell viability in PTEN negative type TNBC cell line (P < 0.0.5).
Merging the identified genes
Identification top hit candidate genes
B
TCGA breast invasive carcinoma (IlluminaHiSeq)
High PTEN
Low PTEN
WDHD1
Significant mRNAs
n=10
n=10
Samples
C
Whole genome siRNA high-throughput screening
PTEN negative
PTEN positive
WDHD1
Significant Genes (Z-score)
n=3
n=3

Figure 2

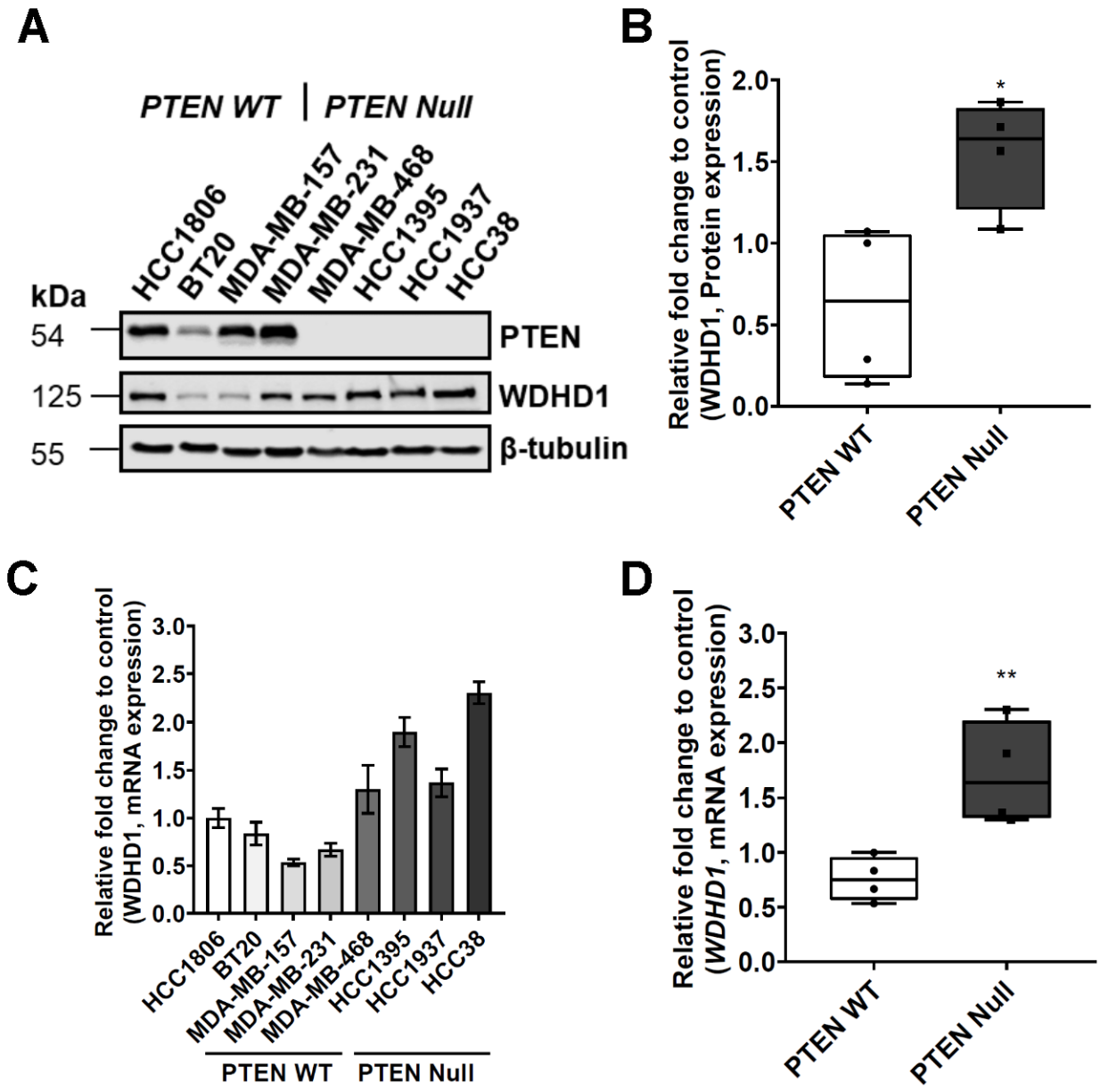
A
PTEN WT | PTEN Null
HCC1806
BT20
MDA-MB-157
MDA-MB-231
MDA-MB-468
HCC1395
HCC1937
HCC38
kDa
54
125
55
PTEN
WDHD1
β-tubulin
B
Relative fold change to control (WDHD1, Protein expression)
2.0
1.5
1.0
0.5
0.0
*
PTEN WT
PTEN Null
C
Relative fold change to control (WDHD1, mRNA expression)
3.0
2.5
2.0
1.5
1.0
0.5
0.0
HCC1806
BT20
MDA-MB-157
MDA-MB-231
MDA-MB-468
HCC1395
HCC1937
HCC38
PTEN WT
PTEN Null
D
Relative fold change to control (WDHD1, mRNA expression)
3.0
2.5
2.0
1.5
1.0
0.5
0.0
**
PTEN WT
PTEN Null

Figure 3

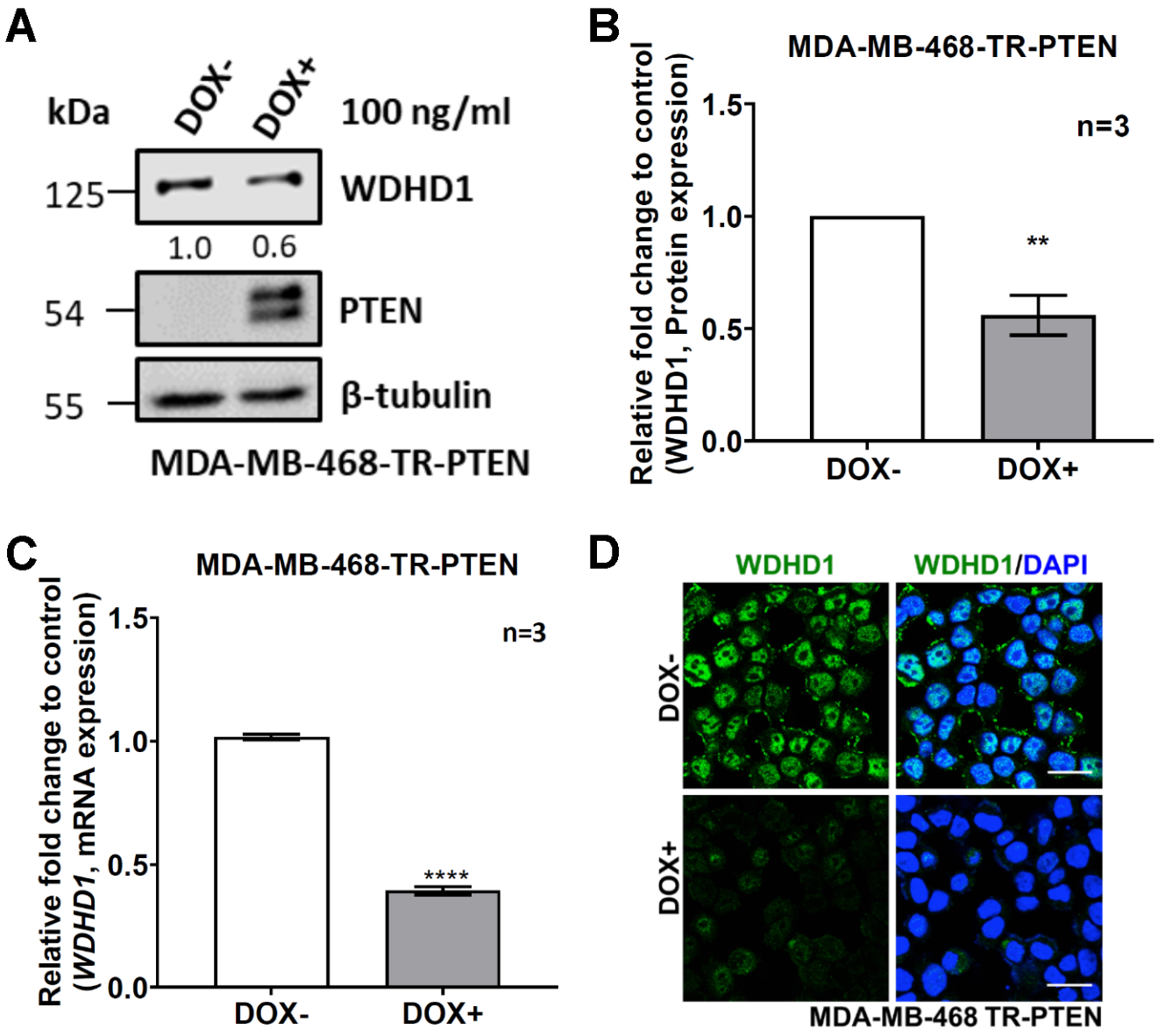
A
kDa
DOX-
DOX+
100 ng/ml
125
WDHD1
1.0
0.6
54
PTEN
55
β-tubulin
MDA-MB-468-TR-PTEN
B
MDA-MB-468-TR-PTEN
n=3
Relative fold change to control
(WDHD1, Protein expression)
1.5
1.0
0.5
0.0
**
DOX-
DOX+
C
MDA-MB-468-TR-PTEN
n=3
Relative fold change to control
(WDHD1, mRNA expression)
1.5
1.0
0.5
0.0
****
DOX-
DOX+
D
WDHD1
WDHD1/DAPI
DOX-
DOX+
MDA-MB-468 TR-PTEN

Figure 4

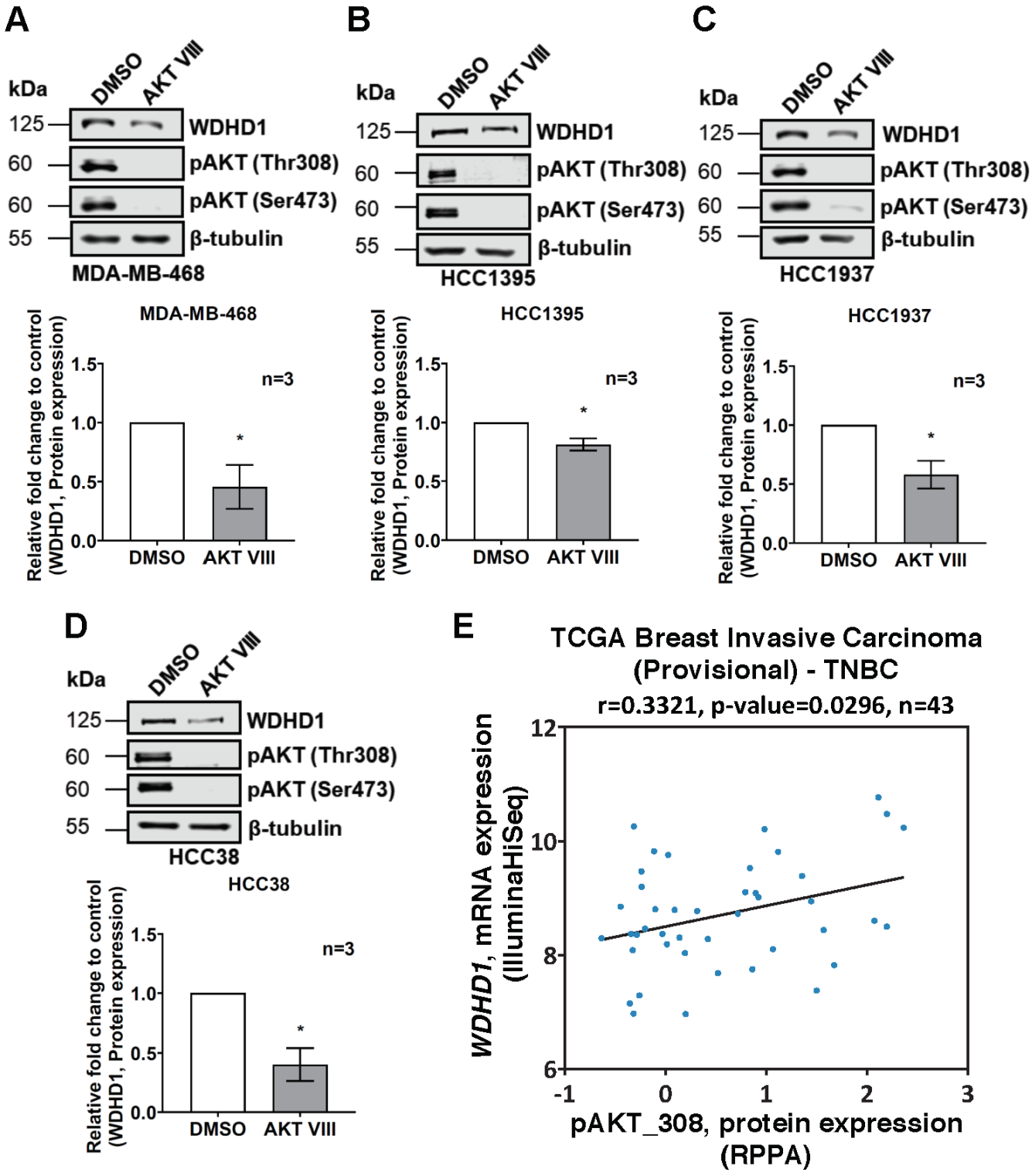
A
B
C
kDa
DMSO
AKT VIII
125
WDHD1
60
pAKT (Thr308)
60
pAKT (Ser473)
55
β-tubulin
MDA-MB-468
HCC1395
HCC1937
Relative fold change to control (WDHD1, Protein expression)
n=3
DMSO
AKT VIII
D
HCC38
E
TCGA Breast Invasive Carcinoma (Provisional) - TNBC
r=0.3321, p-value=0.0296, n=43
WDHD1, mRNA expression (IlluminaHiSeq)
pAKT_308, protein expression (RPPA)

Figure 5

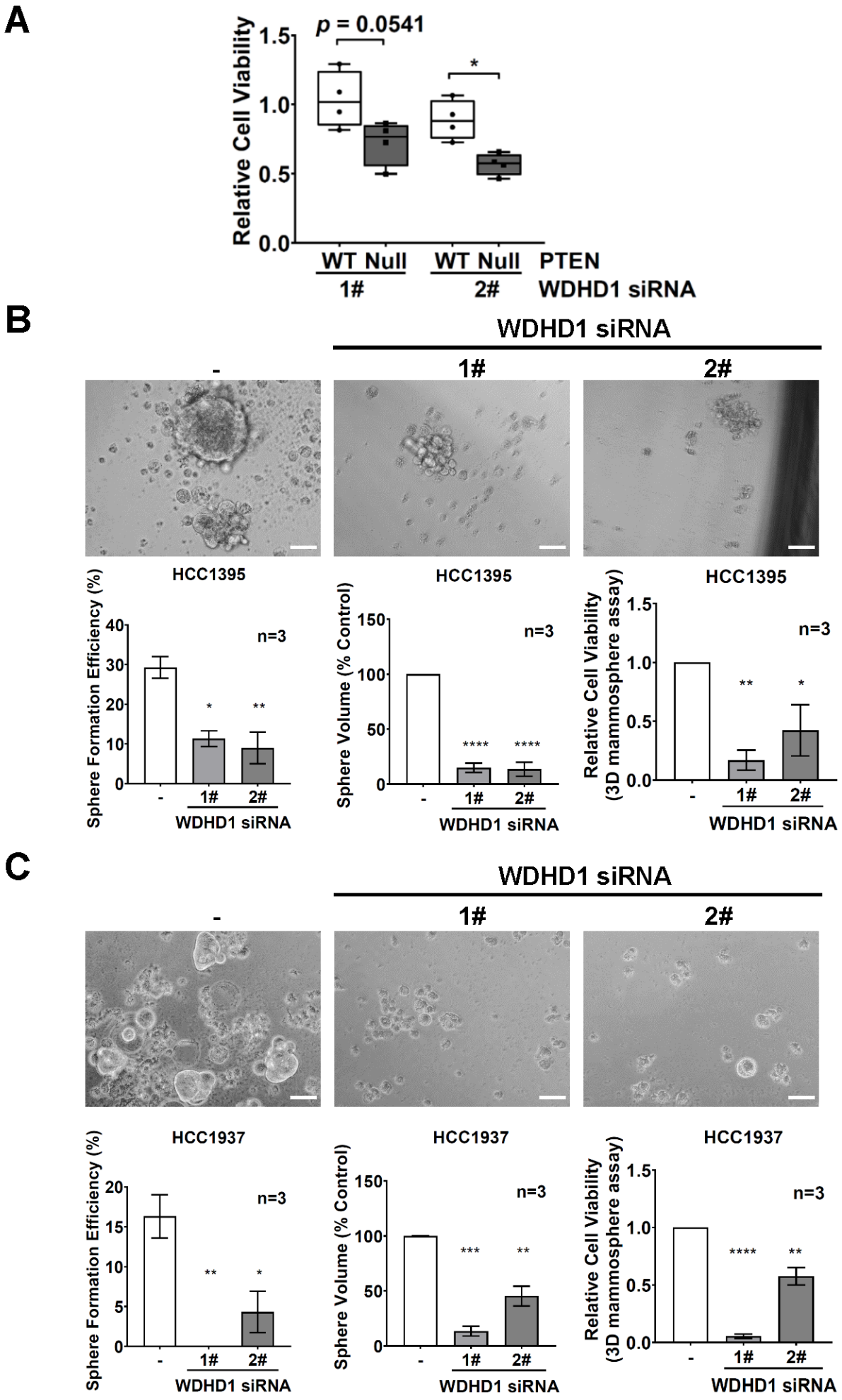
A
p = 0.0541
*
Relative Cell Viability
1.5
1.0
0.5
0.0
WT Null
WT Null
PTEN
1#
2#
WDHD1 siRNA
B
WDHD1 siRNA
-
1#
2#
HCC1395
Sphere Formation Efficiency (%)
40
30
20
10
0
n=3
*
**
-
1#
2#
WDHD1 siRNA
HCC1395
Sphere Volume (% Control)
150
100
50
0
n=3
****
****
-
1#
2#
WDHD1 siRNA
HCC1395
Relative Cell Viability (3D mammosphere assay)
1.5
1.0
0.5
0.0
n=3
**
*
-
1#
2#
WDHD1 siRNA
C
WDHD1 siRNA
-
1#
2#
HCC1937
Sphere Formation Efficiency (%)
20
15
10
5
0
n=3
**
*
-
1#
2#
WDHD1 siRNA
HCC1937
Sphere Volume (% Control)
150
100
50
0
n=3
***
**
-
1#
2#
WDHD1 siRNA
HCC1937
Relative Cell Viability (3D mammosphere assay)
1.5
1.0
0.5
0.0
n=3
****
**
-
1#
2#
WDHD1 siRNA

Figure 6

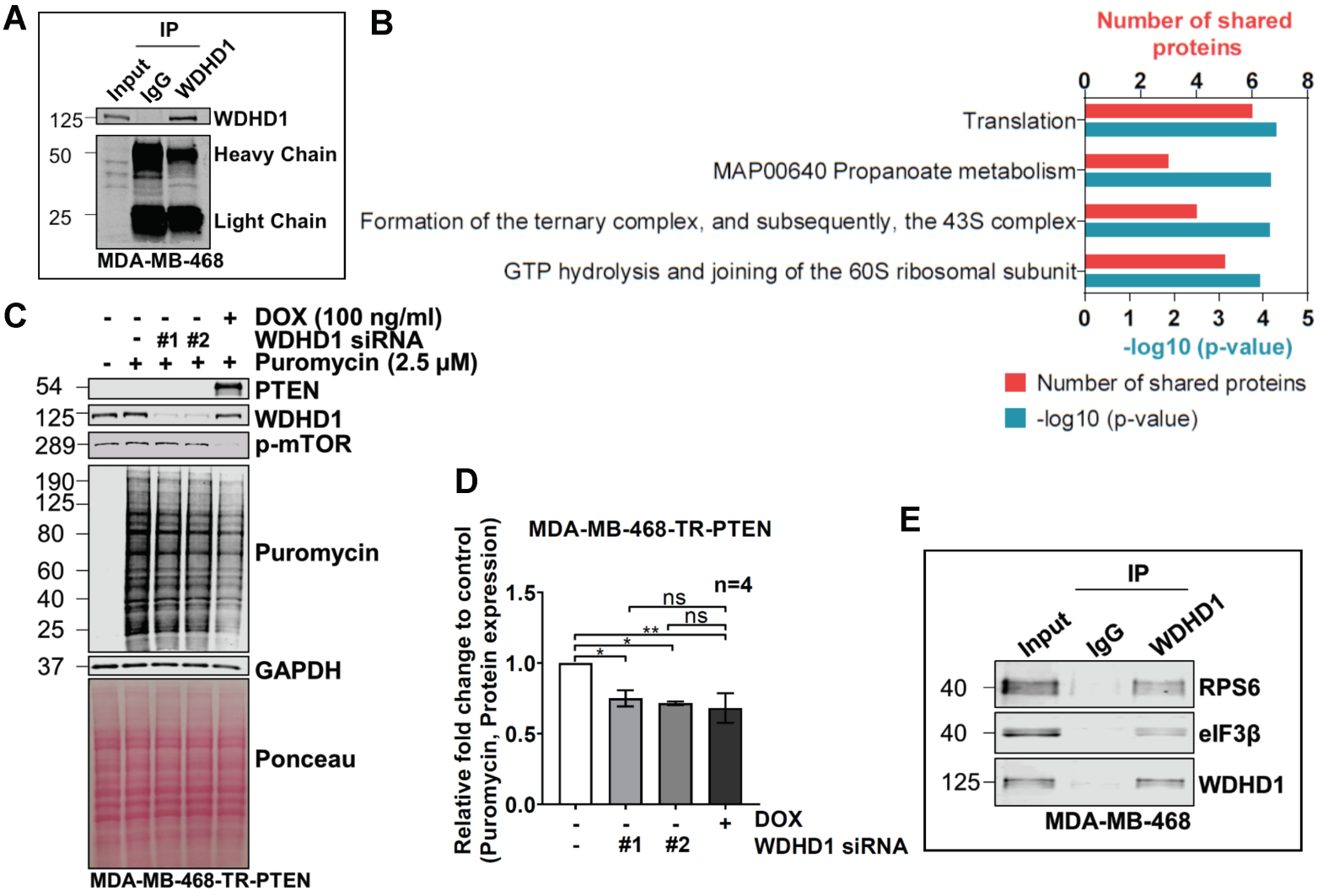
A
IP
Input
IgG
WDHD1
125
WDHD1
50
Heavy Chain
25
Light Chain
MDA-MB-468
B
Number of shared proteins
0 2 4 6 8
Translation
MAP00640 Propanoate metabolism
Formation of the ternary complex, and subsequently, the 43S complex
GTP hydrolysis and joining of the 60S ribosomal subunit
0 1 2 3 4 5
-log10 (p-value)
Number of shared proteins
-log10 (p-value)
C
- - - - + DOX (100 ng/ml)
- #1 #2 WDHD1 siRNA
- + + + + Puromycin (2.5 µM)
54 PTEN
125 WDHD1
289 p-mTOR
190
125
80
60
40
25
Puromycin
37 GAPDH
Ponceau
MDA-MB-468-TR-PTEN
D
MDA-MB-468-TR-PTEN
Relative fold change to control (Puromycin, Protein expression)
1.5
1.0
0.5
0.0
n=4
ns
ns
**
*
*
- - - +
- #1 #2
DOX
WDHD1 siRNA
E
IP
Input
IgG
WDHD1
40 RPS6
40 eIF3β
125 WDHD1
MDA-MB-468

Figure 7

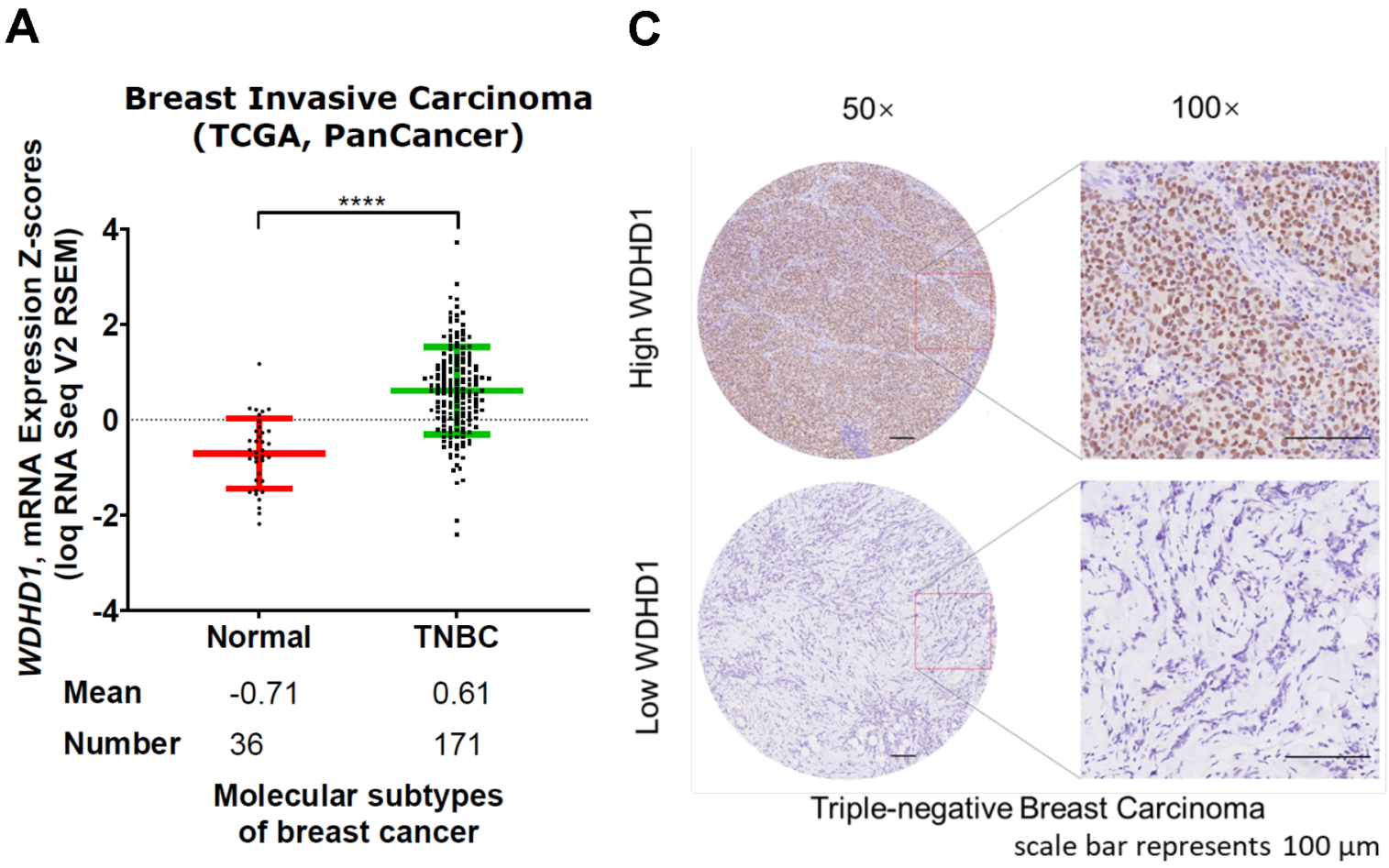
A
Breast Invasive Carcinoma
(TCGA, PanCancer)
****
WDHD1, mRNA Expression Z-scores
(log RNA Seq V2 RSEM)
4
2
0
-2
-4
Normal
TNBC
Mean
-0.71
0.61
Number
36
171
Molecular subtypes
of breast cancer
C
50×
100×
High WDHD1
Low WDHD1
Triple-negative Breast Carcinoma
scale bar represents 100 µm
B
TCGA Breast Invasive Carcinoma
(IlluminaHiSeq) - TNBC
Chi-Square P-value=0.0270
*
≥T2
<T2
Number of patients
15
10
5
0
Low
High
WDHD1
D
r=0.3714, p-value=0.0004, n=88
WDHD1 IHC Score
12
10
8
6
4
2
0
0
20
40
60
80
100
Ki67 (%)

Supplementary Materials

The Cancer Genome Atlas (TCGA) data mining of PTEN

PTEN, mRNA expression Z-scores and PTEN mutation status of breast invasive carcinoma (TCGA, PanCancer) were obtained from the cBioPortal for Cancer Genomics (https://www.cbioportal.org/). *PTEN*, mRNA expression was analysed in each breast cancer molecular subtype along with normal breast samples in GraphPad Prism 8.

Clinical data of breast invasive carcinoma (TCGA, Provisonal) was extracted from the cBioPortal for Cancer Genomics. Molecular subtypes of breast cancer samples were separated based on ER, PR and HER2 status in the clinical data and TNBC samples were extracted.

The two different data sets TCGA_BRCA_RPPA-2015-02-24 for protein expression (RPPA) and TCGA_BRCA_exp_HiSeqV2-2015-02-24 for mRNA expression (IlluminaHiSeq), were extracted from the UCSC Cancer Genome Browser (https://genome-cancer.ucsc.edu/) for the analysis of TNBC samples. TNBC samples in clinical data from the cBioPortal for Cancer Genomics website were aligned with the samples in the TCGA data for both protein and mRNA expression that were extracted from the UCSC Cancer Genome Browser in RStudio (version 3.4.4). Codes are available upon request.

The correlation between PTEN, protein expression in the TCGA protein data (RPPA) and *PTEN*, mRNA expression in the TCGA mRNA expression data (IlluminaHiSeq) was analysed by Pearson's correlation analysis in TNBC samples that were subcategorized from breast invasive carcinoma (TCGA, Provisional).

TCGA breast invasive carcinoma (Protein, RPPA) analysis

Protein (RPPA) TCGA breast invasive carcinoma data from the UCSC Cancer Genome Browser (https://genome-cancer.ucsc.edu/) was obtained that included 410 breast invasive carcinoma samples and 142 proteins. Breast invasive carcinoma samples from the Cancer Genome Browser were aligned with TNBC samples, which were categorised in breast invasive carcinoma (TCGA, Provisional) data. There were 43 common TNBC samples between these two data sets. PTEN, protein expression across the samples was narrowly distributed, samples were grouped as high and low PTEN expressing TNBC samples according to approximately the top 40% and bottom 40% of samples, respectively. The clinical features, tumour size and tumour stage were analysed between the high and low PTEN expressing TNBC samples. The correlation between PTEN and AKT1_PT308 protein expressions (TCGA, RPPA) in TNBC samples that were subcategorized from breast invasive carcinoma (TCGA, Provisional) was analysed by Pearson's correlation analysis.

TCGA breast invasive carcinoma (mRNA, IlluminaHiSeq) analysis

mRNA (IlluminaHiSeq) TCGA breast invasive carcinoma data from the UCSC Cancer Genome Browser (https://genome-cancer.ucsc.edu/) was obtained that included 1,215 breast invasive carcinoma samples and 20,530 mRNAs. Breast invasive carcinoma samples from the Cancer Genome Browser were aligned with TNBC samples, which were categorised in breast invasive carcinoma (TCGA, Provisional) data. There were 92 common TNBC samples between these two data sets. *PTEN*, mRNA expression across the samples was widely distributed. The TNBC samples were grouped into high and low *PTEN* expression based on approximately the top 10% and bottom 10% of samples, respectively. Then, analysis was

performed to find the significantly different mRNAs ($P < 0.05$) between the high and low PTEN groups in RStudio (version 3.4.4). Codes are available upon request.

A whole genome siRNA high-throughput screening and data analysis

To optimise the concentration of doxycycline (DOX), MDA-MB-468-TR-PTEN and MDA-MB-468-TR-EV cell lines were treated with different concentrations of DOX to induce PTEN expression. MCF10A is a non-tumorigenic triple negative breast cell line. PTEN expression was induced with the treatment of DOX in MDA-MB-468-TR-PTEN cell line compared to the DOX untreated cell line (control). No PTEN induction was observed with the treatment of DOX in MDA-MB-468-TR-EV cell line. Similar levels of PTEN induction were observed with different concentrations of DOX, comparable to the endogenous PTEN expression in MCF10A cells (Fig. S2a). In the following studies, we used 100 ng/ml DOX to induce PTEN in MDA-MB-468-TR-PTEN cells. As expected, PTEN induction led to reduced levels of phospho-AKT (p-AKT), but not phospho-ERK (p-ERK) (Fig. S2a).

To fluorescently label MDA-MB-468-TR-PTEN and MDA-MB-468-TR-EV cells, pCherryFP-N1 and p-EGFP-N1 were stably transfected into them, respectively. Single clones were picked and sorted by fluorescence-activated cell sorting (FACS), and named as MDA-MB-468-TR-PTEN/CherryFP or MDA-MB-468-TR-EV/GFP (Fig. S2b).

The human siGENOME siRNA library - Genome (G-005005) was obtained from Dharmacon. siRNA transfection experiments were performed in 96-well format in antibiotic-free medium, using a reverse transfection employing 25 nM siRNA and 0.15 μl Dharmafect 2 (Dharmacon) per well together with a starting cell density optimized to produce an 80% confluent monolayer in mock-treated cells at the conclusion of the experiment. DOX-treated MDA-MB-468-TR-PTEN/CherryFP (PTEN+) or MDA-MB-468-TR-EV/GFP (PTEN-) cells were mixed and transfected at a 1:1 ratio in 96-well plates. Cells were fixed with 4%

paraformaldehyde at 96 h post transfection. CherryFP or GFP fluorescence was read on an EnVision 2102 Plate-reader (Perkin-Elmer) to evaluate cell numbers in PTEN+ or PTEN- cells, respectively (Fig. S2c). Overall, four patterns were observed, including "No effects", "Non-selective cytotoxic", "Cytotoxic hits for PTEN+" and "Cytotoxic hits for PTEN-" (Fig. S2c).

The whole genome siRNA screen data contained siRNAs targeting 21,121 genes in two cell lines expressing GFP fluorescence (PTEN-) or red fluorescence (PTEN+), respectively. Each group contained three biological repeats, showing reproducible results (Pearson's correlation (r) = 0.8 and $P < 0.001$) (Fig. S3a). We identified 4,647 genes that have differential effects between PTEN- and PTEN+ expressing cells ($P < 0.05$), which were shown in a heat-map (Fig. S3b).

Identification of top hit genes

The statistically different mRNAs in the TCGA (IlluminaHiseq) data set that were highly expressed in the low PTEN TNBC group were merged with statistically different genes in the whole genome siRNA screening data set, which showed a decrease in cell viability in PTEN- TNBC cell line group by using RStudio (version 3.4.4) to identify the top hit candidate gene(s).

TCGA data mining with identified top hit gene, *WDHD1*

WDHD1, mRNA expression Z-scores of breast invasive carcinoma (TCGA, PanCancer) were obtained from the cBioPortal for Cancer Genomics. *WDHD1*, mRNA expression was analysed between the normal breast and TNBC samples in GraphPad Prism 8.

WDHD1, mRNA expression of subcategorized-TNBC samples using clinical data (TCGA, Provisional) was extracted from the TCGA breast invasive carcinoma (IlluminaHiSeq) data set. Approximately the top 10% and bottom 10% of TNBC samples were chosen for the high and low *WDHD1*, mRNA expression in IlluminaHiSeq data. Then, significantly different mRNAs were identified between the high *vs.* low *WDHD1* groups in RStudio (version 3.4.4), $P < 0.05$. Tumour size of TNBC samples from the clinical data (TCGA, Provisional) was extracted and analysed between the low and high *WDHD1*, mRNA expression.

Sample preparations for mass spectrometry

Protein G Sepharose beads (GE Healthcare) were re-suspended in 100 µL of 100 mM ammonium bicarbonate containing 0.25% Rapigest (Waters Corporation), heated at 70°C for 60 min, centrifuged at 13,000 x g for 5 min and the supernatant was collected. Proteins extracts were reduced with 0.5 µg DTT for 1 h and then alkylated with 2.5 µg IAA for 45 min in the dark, and digested with 0.5 µg sequencing grade modified trypsin (1/50 (w/w)) overnight at 37°C. Samples were acidified with 1% trifluoroacetic acid (v/v), centrifuged at 13,000 x g for 5 min and the supernatant collected. Supernatants were lyophilized and re-suspended in 20 µL of buffer A (0.1% formic acid in water (v/v)) prior to mass spectrometry.

Mass spectrometry and database search

18 µL of peptide extracts in buffer A were separated on an Ultimate 3000 RSLC nano system, (Thermo Scientific), using a PepMap C18 EASY-Spray LC column, 2 µm particle size, 75 µm x 75 cm column, (Thermo Scientific), over a 140 min (single run) linear gradient of 3–25% buffer B (0.1% formic acid in acetonitrile (v/v)) in buffer A (0.1% formic acid in water (v/v)) at a flow rate of 300 nL/min. Peptides were introduced using an EASY□Spray source

at 2000 V to a Fusion Tribrid Orbitrap mass spectrometer, (Thermo Scientific). The ion transfer tube temperature was set to 275°C. Full MS spectra were recorded from 300 to 1500 m/z in the Orbitrap at 120,000 resolution with an automatic was performed using TopSpeed mode at a cycle time of 3 s. Peptide ions were isolated using an isolation width of 1.6 amu and trapped at a maximal injection time of 120 ms with an AGC target of 300,000. Higher energy collisional dissociation (HCD) fragmentation was induced at an energy setting of 28 for peptides with a charge state of 2–4. Fragments were analysed in the orbitrap at 30,000 resolution.

Analysis of raw data was performed using Proteome Discoverer software (Thermo Scientific), and the data processed to generate reduced charge state and deisotoped precursor and associated product ion peak lists. These peak lists were searched against the Human protein database. A maximum of one missed cleavage was allowed for tryptic digestion and the variable modification was set to contain oxidation of methionine and N-terminal protein acetylation. Carboxyamidomethylation of cysteine was set as a fixed modification. The false discovery rate (FDR) was estimated with randomized decoy database searches and were filtered to 1% FDR.

Supplementary Figure Legends

Figure S1. TCGA analysis confirms PTEN expression is decreased in TNBC and correlates with clinical stages.

a Graph showing mRNA levels (Z-scores) of *PTEN* in the TCGA samples from normal breast (*n* = 36), luminal A (*n* = 499), luminal B (*n* = 197), HER2+ (*n* = 78) and TNBC (*n* = 171). Data are mean ± SD. ****$P < 0.0001$. **b** The scatter plot for the correlation of TNBC samples between PTEN, protein expression (RPPA) and *PTEN*, mRNA expression (IlluminaHiSeq) in the TCGA breast invasive carcinoma (Pearson's correlation (r) = 0.5504; $P = 0.0001$). **c** Graph showing the number of TNBC patients (TCGA) with T2 and above or < T2 in the low or high PTEN group. Statistical significance was determined by $\chi 2$ analysis. *$P < 0.05$. **d** Graph showing the number of TNBC patients (TCGA) with Stage II and above or Stage I in the low or high PTEN group. Statistical significance was determined by $\chi 2$ analysis. *$P < 0.05$. **e** The scatter plot for the correlation of TNBC samples between PTEN, protein expression (RPPA) and AKT1_PT308, protein expression (RPPA) in the TCGA breast invasive carcinoma (Protein, RPPA) data (Pearson's correlation (r) = -0.5478; $P = 0.0001$). **f** Heat-map showing 3,009 significantly different mRNAs between the high and low *PTEN* expressing TNBC samples obtained from the TCGA analysis. Red indicates up-regulation and blue for down-regulation. *n* = 10 per group.

Figure S2. Workflow showing the whole genome siRNA screen in isogenic PTEN positive or negative TNBC cells.

a Protein expressions of PTEN, phospho-AKT (p-AKT), AKT, phospho-ERK (p-ERK) and ERK expression in MCF10A, MDA-MB-468-TR-PTEN and MDA-MB-468-TR-EV with indicated treatments. GAPDH was used as a loading control. **b** A schematic diagram

showing fluorescently labelling of MDA-MB-468-TR-PTEN and MDA-MB-468-TR-EV cells. Plasmids pCherryFP-N1 or p-EGFP-N1 were stably transfected into these two cell lines, respectively. Single clones were picked and sorted by fluorescence-activated cell sorting (FACS), and named as MDA-MB-468-TR-PTEN/CherryFP or MDA-MB-468-TR-EV/GFP. **c** A schematic diagram showing the whole genome siRNA screen in PTEN+ and PTEN- cell lines. DOX-treated MDA-MB-468-TR-PTEN/CherryFP (PTEN+) or MDA-MB-468-TR-EV/GFP (PTEN-) cells were mixed and transfected at a 1:1 ratio in 96-well plates. Cells were fixed with 4% paraformaldehyde at 96 h post transfection. Fluorescence was read on an EnVision 2102 Plate-reader.

Figure S3. Candidate genes essential for the survival of PTEN-inactive TNBC cells are identified by a whole genome siRNA screen.

a The response of cell lines to 21,121 siRNA pools in 3 replicate screens based on Z-scores was analysed by Pearson's correlation. Individual dot indicates the pool of siRNA. Top and bottom panels show reproducibility analysis between the replicates in PTEN- cells and PTEN+ cells, respectively. **b** Heat-map showing 4,647 genes that have significant decrease in cell viability between PTEN+ and PTEN- TNBC cells obtained from the whole genome siRNA screen. Red indicates the high Z-scores and blue for low Z-scores. $n = 3$ per group.

Figure S4. WDHD1 is required for the survival of PTEN null TNBC cells cultured in 2D. Protein expression of WDHD1 in HCC1806 (**a**), BT20 (**b**), MDA-MB-157 (**c**), MDA-MB-231 (**d**), MDA-MB-468 (**e**), HCC1395 (**f**), HCC1937 (**g**) and HCC38 (**h**) with indicated transfections in 2D cultures. β-tubulin was used as a loading control. Graphs showing relative cell viability in HCC1806 (**a**), BT20 (**b**), MDA-MB-157 (**c**), MDA-MB-231 (**d**), MDA-MB-

468 (**e**), HCC1395 (**f**), HCC1937 (**g**) and HCC38 (**h**) with indicated transfections cultured in 2D cultures. Cell-Titer Glo® assay was performed to measure cell viability. Data are mean ± SEM. $n = 3$ per group. *$P < 0.05$. ** $P < 0.01$.

Figure S5. WDHD1 is required for the survival of PTEN null TNBC cells cultured in 3D.

Representative phase contrast microscopy images of PTEN WT TNBC cell line BT20 (**a**) or MDA-MB-231 (**b**) with indicated transfections cultured in 3D. Scale bar: 50 μm. Graphs showing sphere formation efficiency, sphere volume and cell viability (Cell-Titer Glo® assay) in BT20 (**a**) or MDA-MB-231 (**b**) with indicated transfections cultured in 3D. Data are mean ± SEM. $n = 3$ samples per group. *$P < 0.05$.

Figure S6. TCGA analysis suggests an important role of WDHD1 in cell cycle regulation.

(**a**) Heat-map showing differentially expressed genes (DEGs) in TNBC samples with the low *WDHD1* compared to those with the high WDHD1 obtained from the TCGA analysis. Red indicates up-regulation and blue for down-regulation. $n = 10$ per group. (**b**) Functional enrichment (ToppGene) of up-regulated DEGs in the high WDHD1 group was visualised on a bar chart, showing number of shared mRNAs (genes) and -Log10 (*P* value).

Figure S7. Essential roles of WDHD1 in cell cycle in PTEN null TNBC cell lines.

Protein expression of WDHD1 in MDA-MB-468 (**a**), HCC1395 (**b**), BT20 (**c**) and MDA-MB-231 (**d**) with indicated transfections. β-tubulin was used as a loading control. Representative flow cytometry histograms of percentage of cells in G1, S and G2/M phases of cell cycle from MDA-MB-468 (**a**) or HCC1395 (**b**) with indicated transfections. Graphs

showing the percentage of cells in S-phase from MDA-MB-468 (**a**) or HCC1395 (**b**) with indicated transfections. In **c** and **d**, graphs showing the percentage of cells in G1, S or G2/M phases from BT20 (**c**) and MDA-MB-231 (**d**) with indicated transfections. Data are mean ± SEM. $n = 3$ samples per group. *$P < 0.05$. **$P < 0.01$.

Supplementary Figure 1

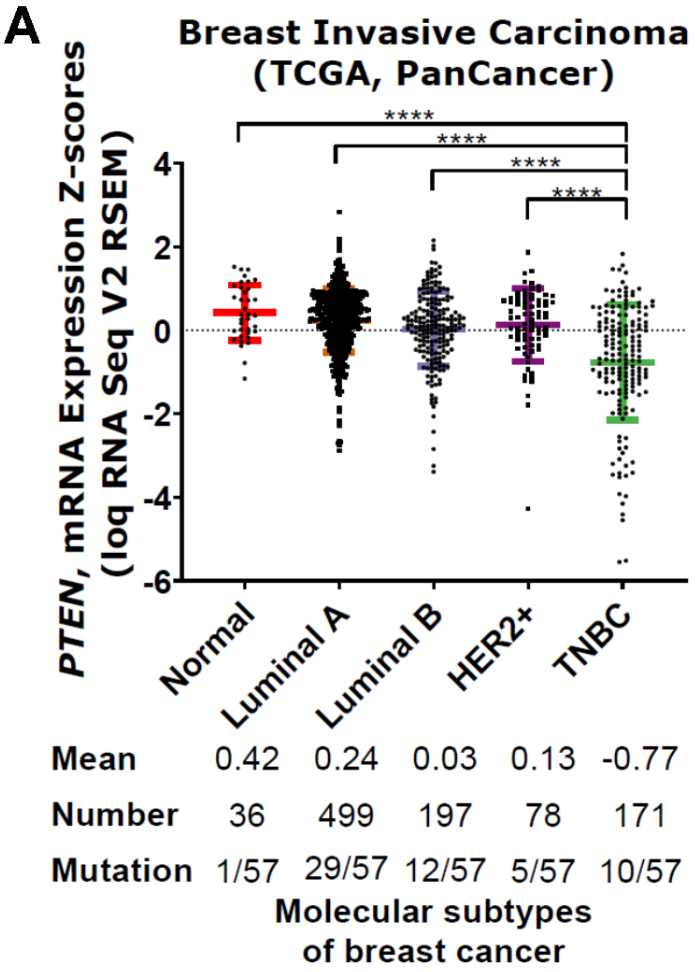

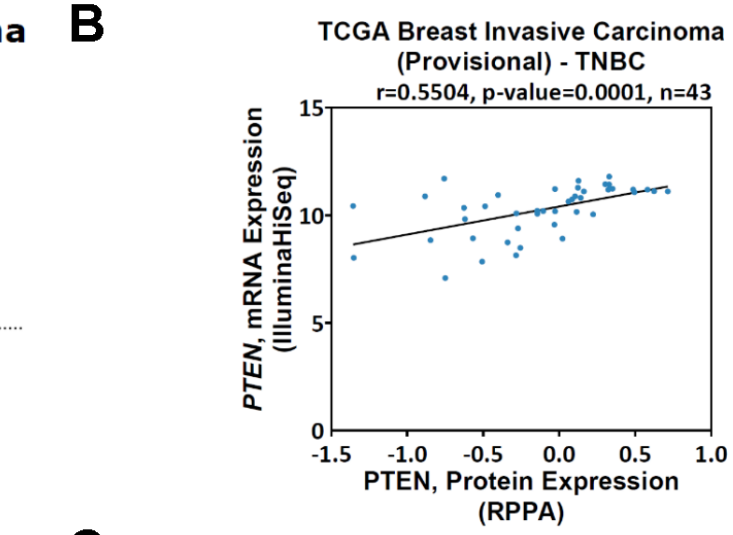

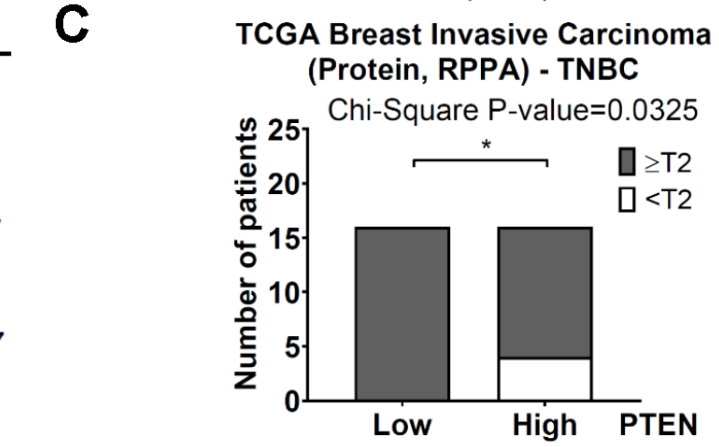

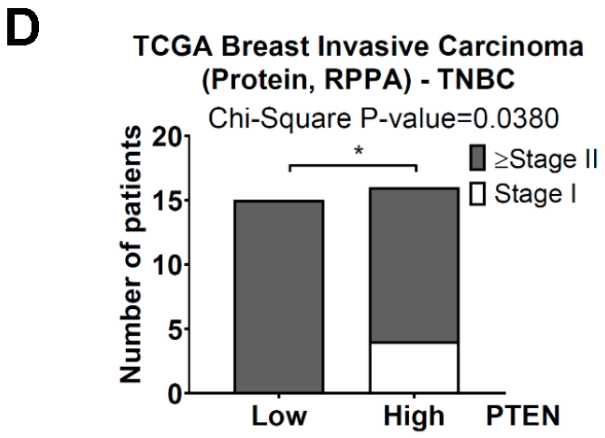

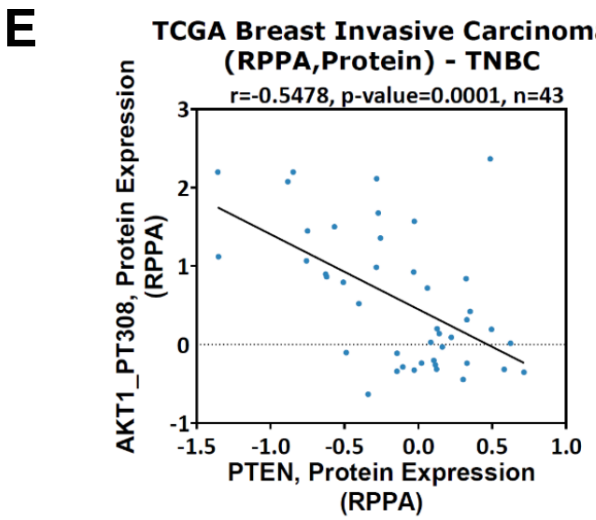

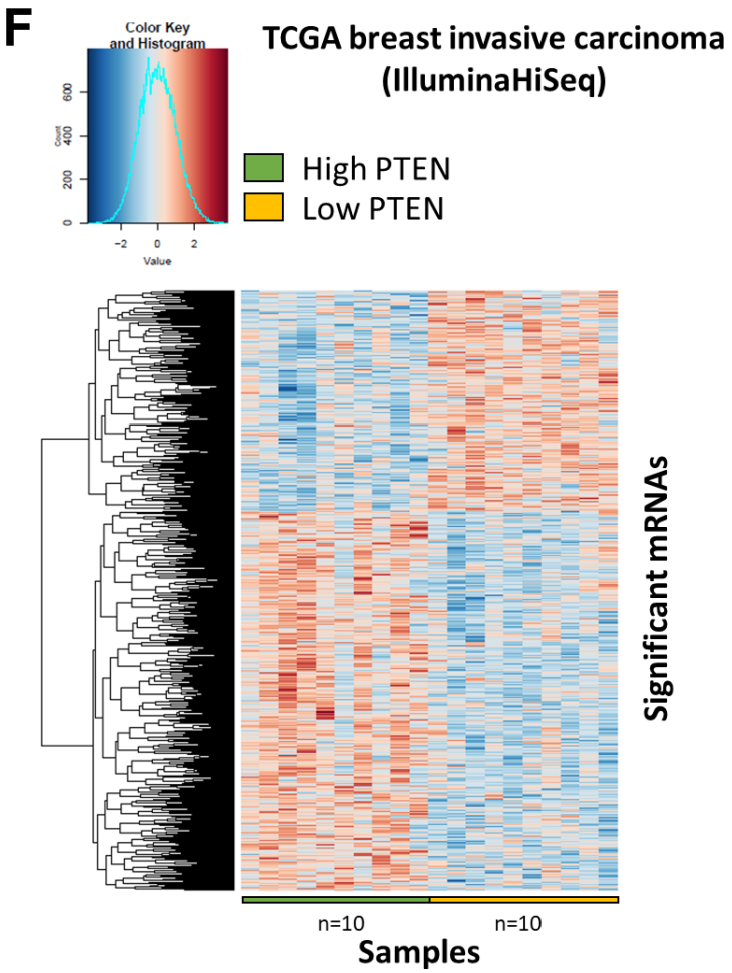

Supplementary Figure 2

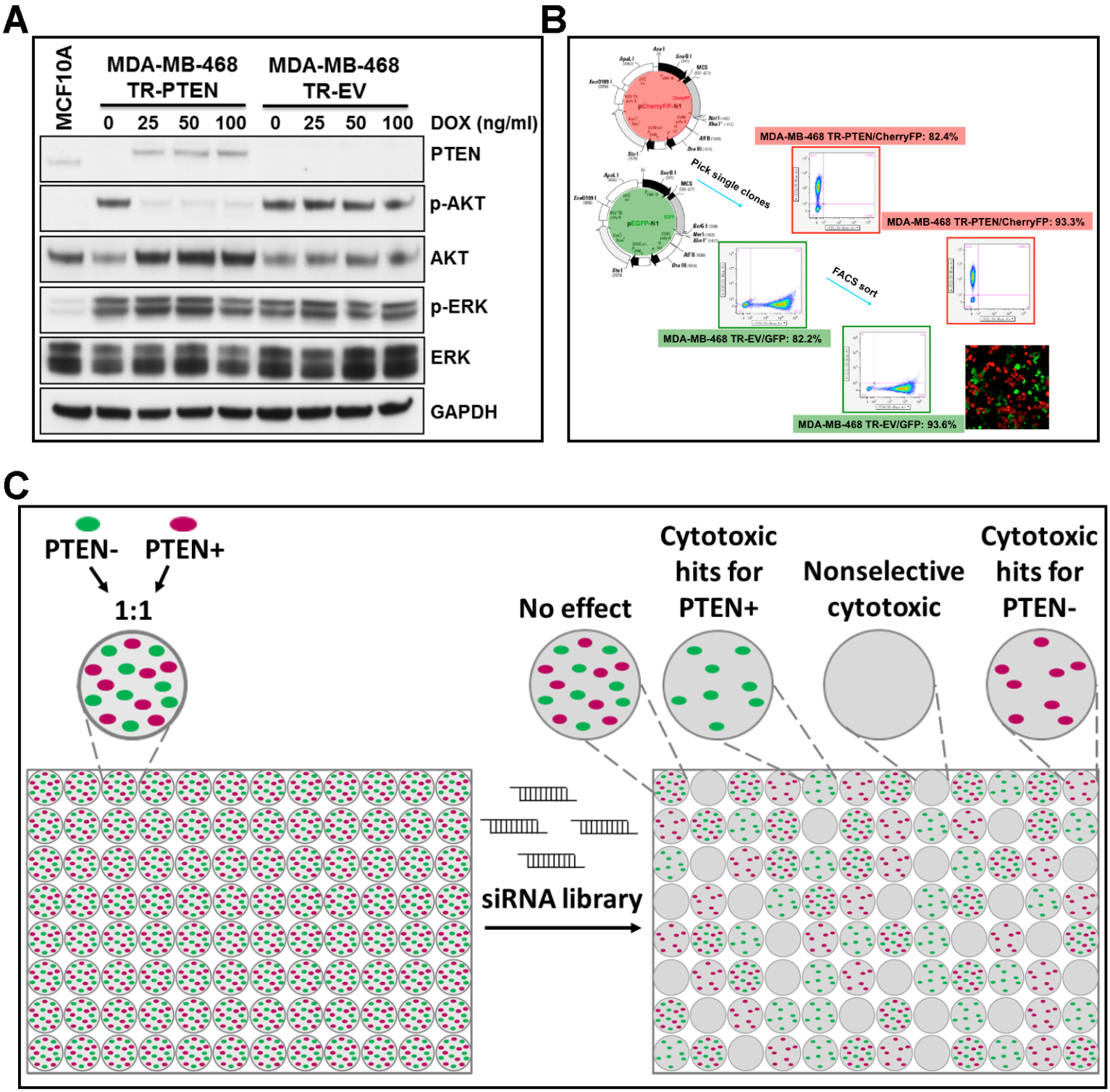

Supplementary Figure 3

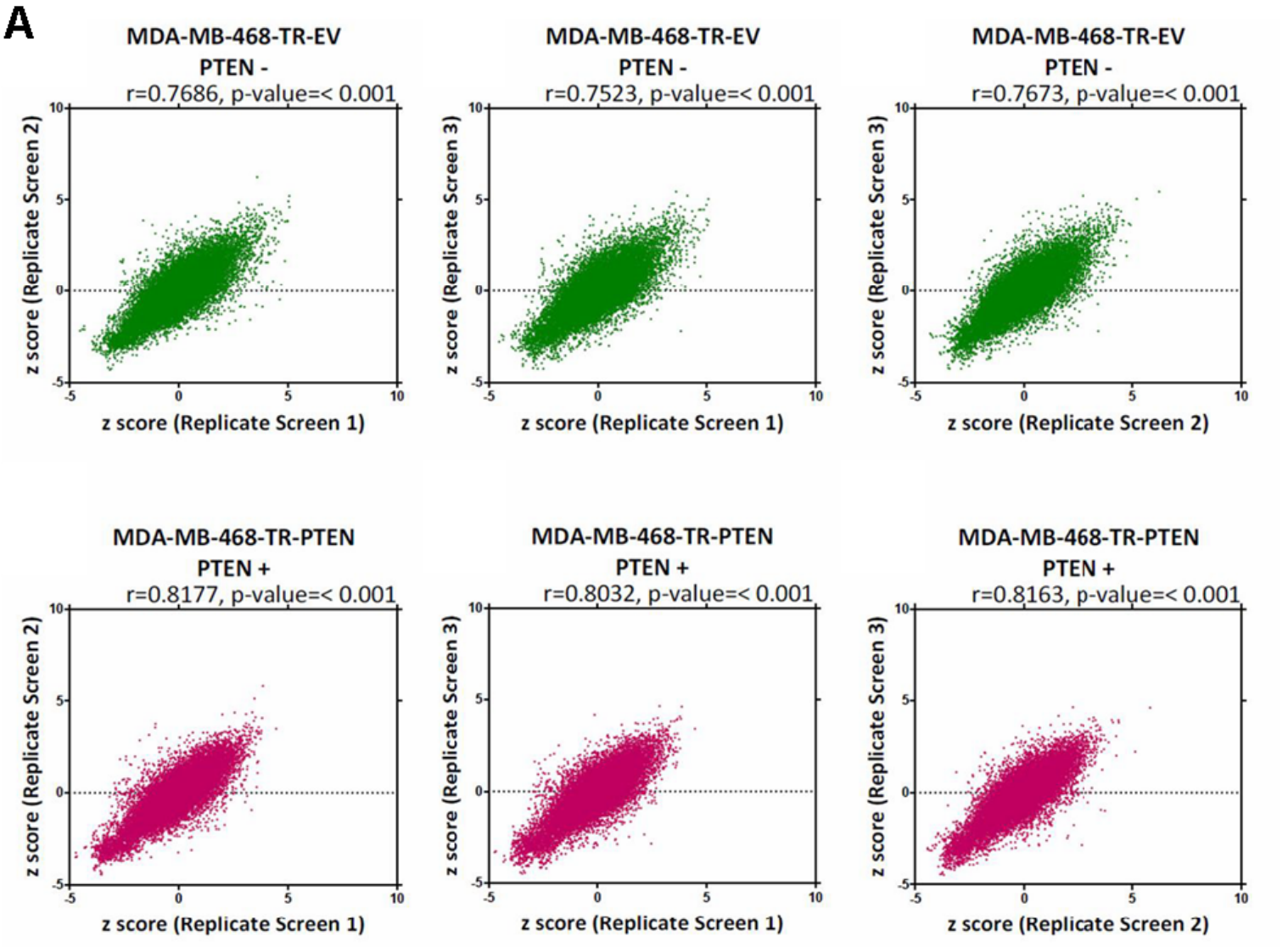

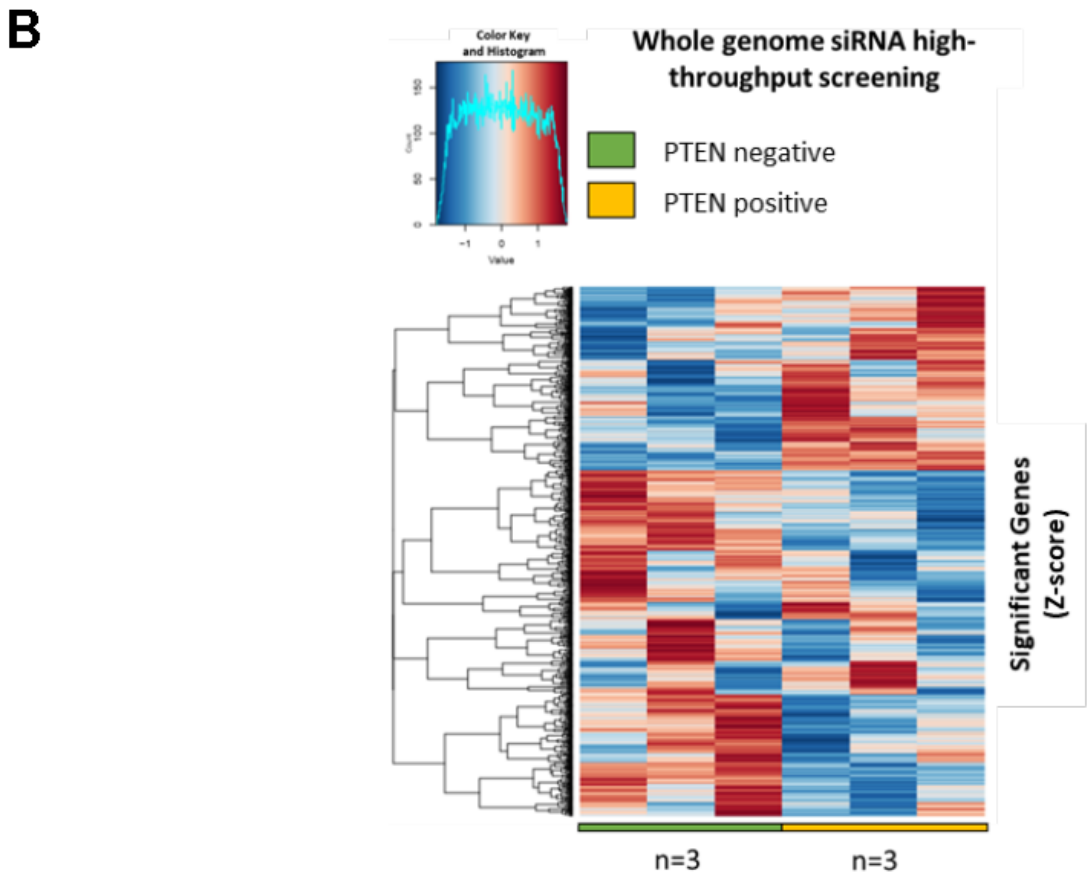

Supplementary Figure 4

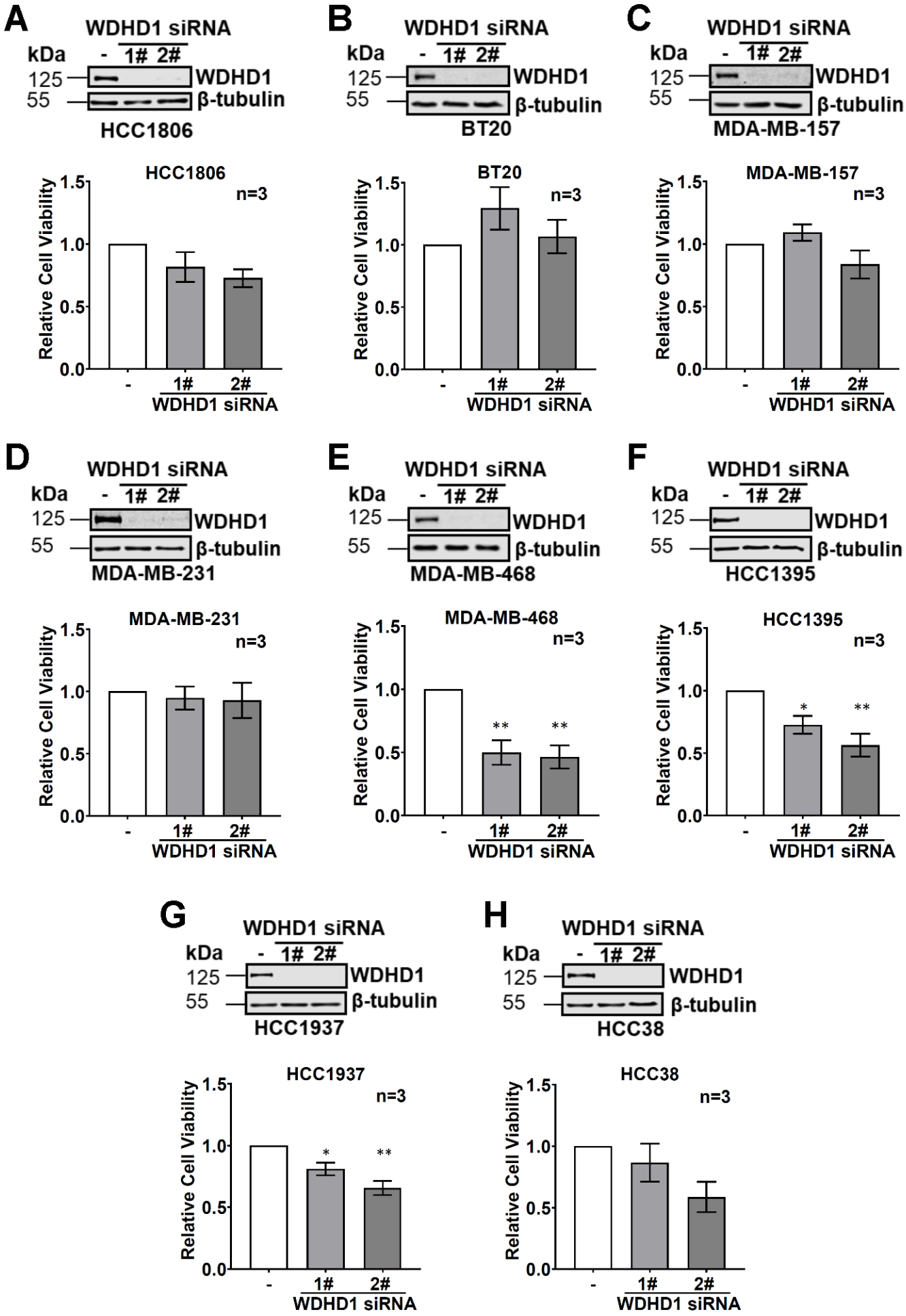

Supplementary Figure 5

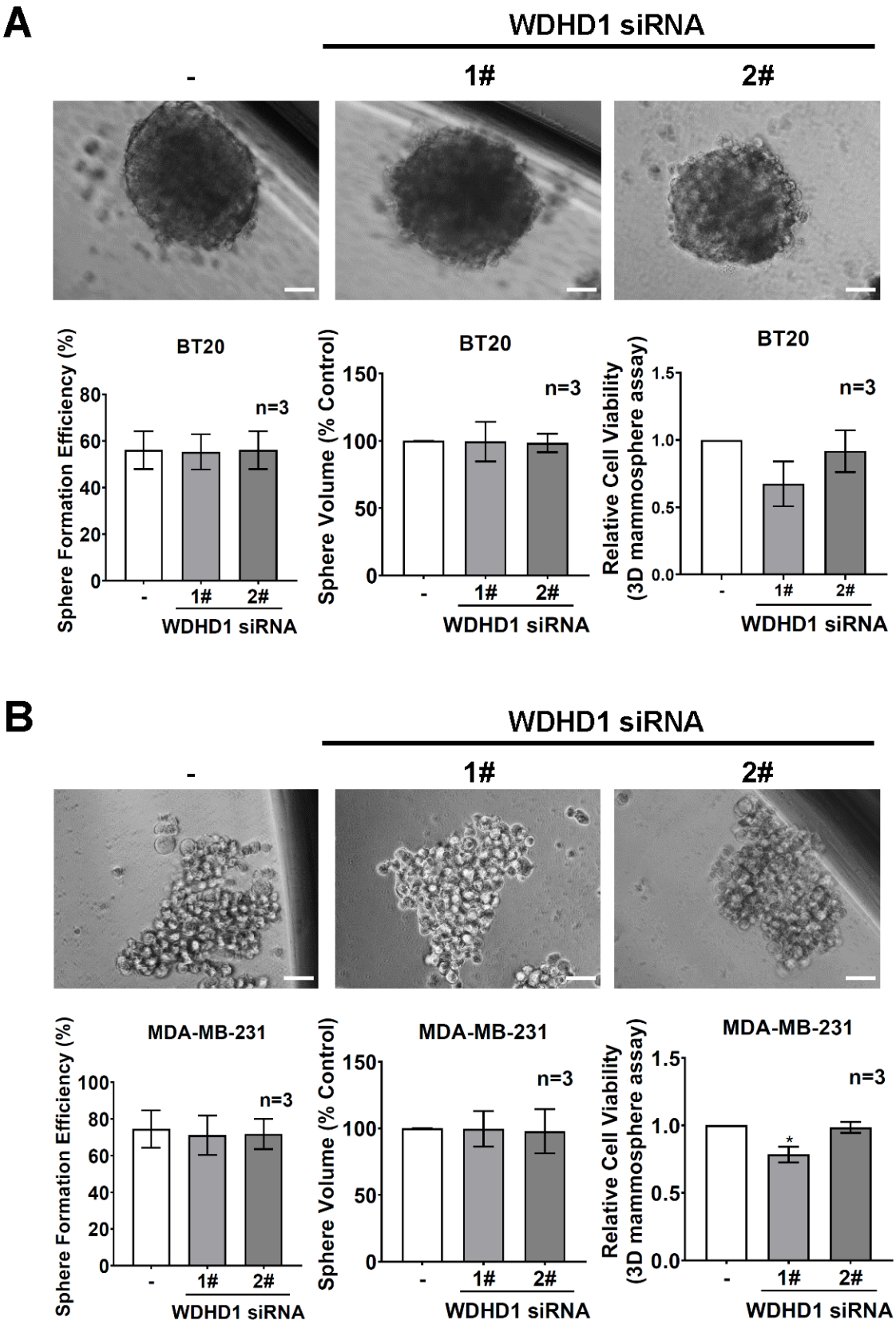

Supplementary Figure 6

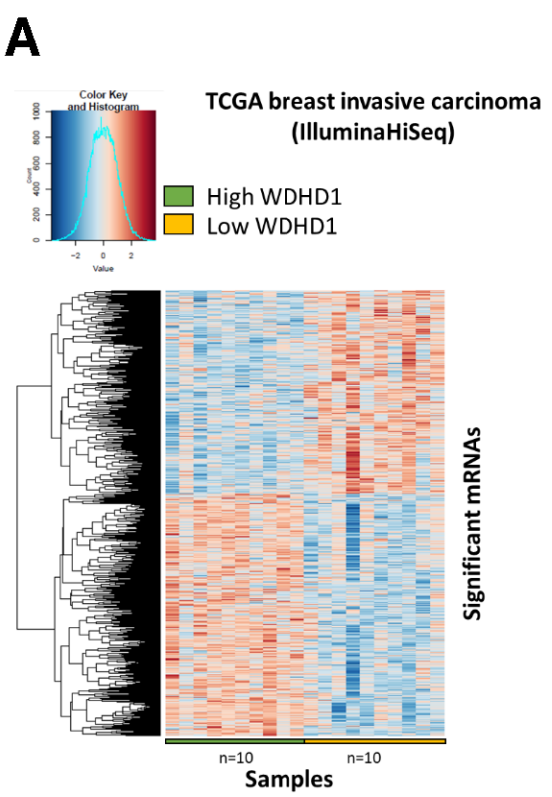

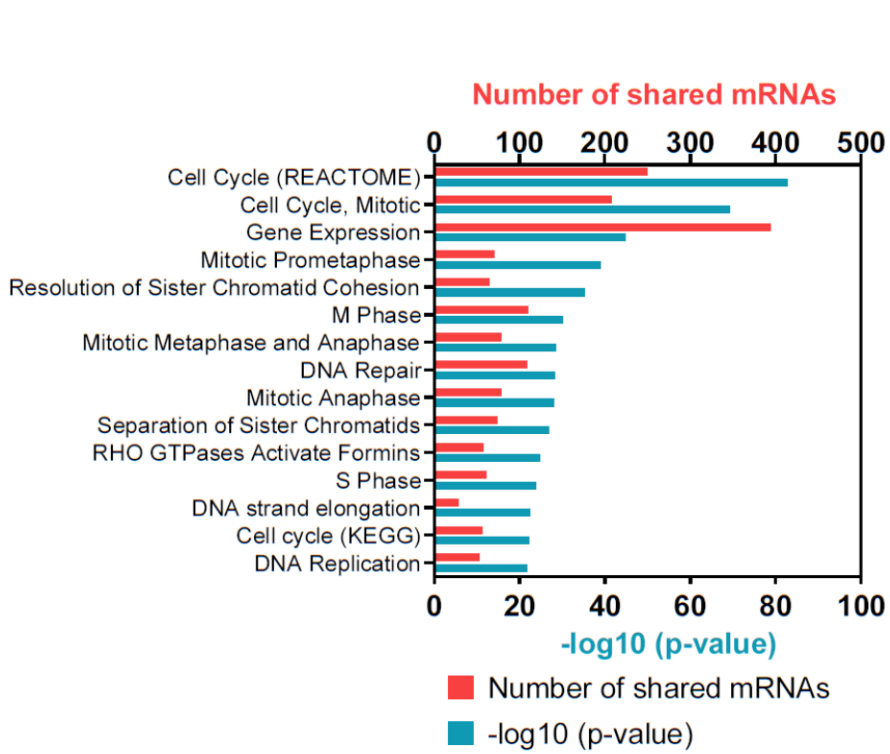

Supplementary Figure 7

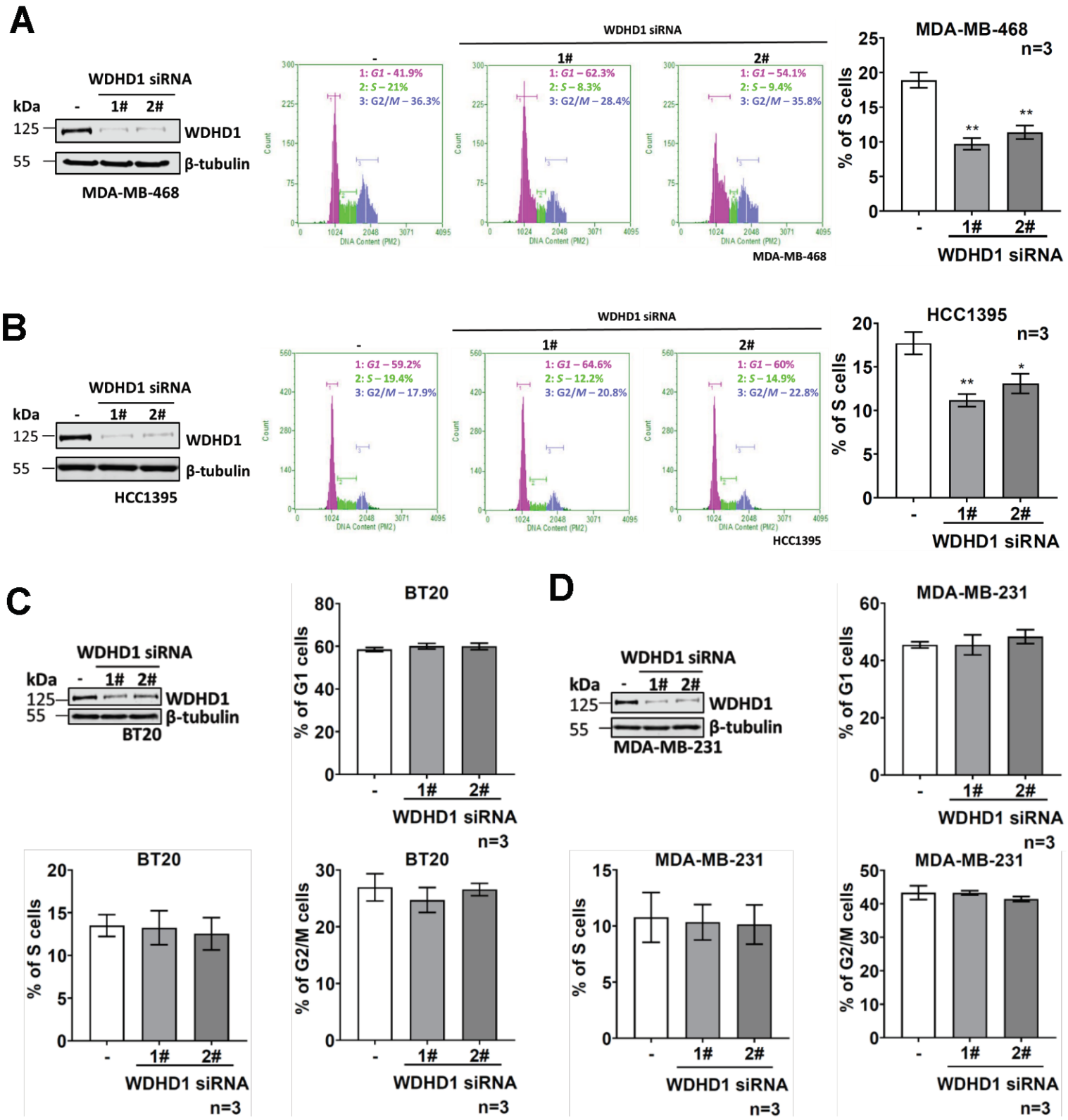

Supplementary Tables

Table S1. Expressions of 47 candidate mRNAs essential for the survival of PTEN-inactive TNBC cells in the TCGA samples with the high *vs.* low PTEN.

Table S2. 47 candidate genes essential for the survival of PTEN-inactive TNBC cells are identified by a whole genome siRNA screen.

Table S3. Functional enrichment (ToppGene) of WDHD1 binding partners identified via IP-MS.

Table S1.
Expressions of 47 candidate mRNAs essential for the survival of PTEN-inactive TNBC cells in TCGA samples with high vs. low PTEN.

mRNAs	High PTEN	Low PTEN	p-value	Fold change (Low PTEN *vs.* High PTEN)
ONECUT2	3.330307692	5.528269231	0.015762538	2.197961538
RAC3	7.164069231	8.712976923	0.000187418	1.548907692
MT3	0.831292308	2.281823077	0.004398609	1.450530769
KCNK12	1.683515385	3.062869231	0.034701609	1.379353846
IL27RA	8.972453846	10.33356154	0.027588268	1.361107692
ZNF572	4.763353846	6.107707692	0.039865878	1.344353846
LOC92659	5.834553846	7.089246154	0.037744031	1.254692308
INCENP	8.738876923	9.826923077	0.001714845	1.088046154
LRFN4	8.515830769	9.576861538	0.015227389	1.061030769
SQLE	9.968030769	10.92553077	0.02285627	0.9575
CHEK2	8.091992308	9.038753846	0.002980991	0.946761538
TRIB1	10.32734615	11.25185385	0.010144165	0.924507692
TAPBPL	8.767253846	9.626730769	0.048659343	0.859476923
DONSON	8.591876923	9.408430769	0.007667299	0.816553846
WDHD1	8.093561538	8.900830769	0.031434154	0.807269231
STRA13	8.766123077	9.5198	0.041809581	0.753676923
POLA2	8.740423077	9.491853846	0.000314807	0.751430769
PDE7A	10.44486923	11.17157692	0.02372454	0.726707692
CCT6A	12.20083846	12.88191538	0.001231252	0.681076923
FANCL	8.505107692	9.185792308	0.007778904	0.680684615
ATP5C1	11.94586923	12.6111	0.028513783	0.665230769
SEPHS1	10.7076	11.37118462	0.011911934	0.663584615
TIMELESS	9.805730769	10.46882308	0.011253392	0.663092308
MRPS9	9.197369231	9.820261538	0.03839716	0.622892308
RPN2	12.97282308	13.59485385	0.011910491	0.622030769
TIMM17A	10.4507	11.06684615	0.021730113	0.616146154
AACS	9.457523077	10.06505385	0.033455447	0.607530769
COMMD1	8.031492308	8.638923077	0.009173403	0.607430769
IMPDH1	10.44752308	11.00871538	0.01530917	0.561192308
NCBP2	10.9419	11.44153077	0.032617826	0.499630769
CLNS1A	10.82855385	11.32215385	0.038434893	0.4936
RPN1	12.93968462	13.41123077	0.012294958	0.471546154
TNKS1BP1	12.03065385	12.49049231	0.013810087	0.459838462
WBP11	11.05110769	11.50984615	0.032340999	0.458738462
SNRPC	10.44247692	10.89676923	0.020849254	0.454292308
PRPF18	8.959615385	9.406792308	0.017312774	0.447176923
STRBP	9.945215385	10.38250769	0.046378082	0.437292308
ADCK1	7.059492308	7.471923077	0.037393275	0.412430769
SIP1	7.260353846	7.641869231	0.045023179	0.381515385
COPS3	10.02273846	10.40316154	0.041841487	0.380423077
ADSL	9.878215385	10.25072308	0.029475435	0.372507692
EIF2B5	10.2587	10.54596923	0.039223291	0.287269231

Table S2.
47 candidate genes essential for the survival of PTEN-inactive TNBC cells are identified by a whole genome siRNA screen.

Genes	PTEN negative	PTEN positive	p-value	ΔZ Score (PTEN positive - PTEN negative)
WBP11	-0.416666667	1.514	0.003782644	1.930666667
SQLE	1.024333333	2.385333333	0.000762673	1.361
ZNF572	-0.858666667	0.421666667	0.031505249	1.280333333
MT3	-0.134	1.144333333	0.035554253	1.278333333
KCNK12	-0.923333333	0.298333333	0.027761125	1.221666667
DONSON	-0.618333333	0.521333333	0.002206531	1.139666667
RAC3	0.546	1.680666667	0.044216827	1.134666667
MRPS9	-0.344	0.786333333	0.017007419	1.130333333
ATP5C1	-0.069	1.061	0.013828186	1.13
TIMM17A	0.634666667	1.711333333	0.006612039	1.076666667
FANCL	0.013333333	1.018	0.037311343	1.004666667
TAPBPL	0.252333333	1.221666667	0.009058102	0.969333333
WDHD1	-1.258333333	-0.316666667	0.00910254	0.941666667
NCBP2	-0.447333333	0.456	0.025800729	0.903333333
LOC92659	0.307333333	1.199	0.013386486	0.891666667
IMPDH1	-0.101666667	0.740333333	0.014808154	0.842
RPN1	-0.001666667	0.825	0.042232145	0.826666667
SNRPC	-0.074	0.693	1.42E-05	0.767
ADCK1	0.386666667	1.132666667	0.045399218	0.746
PRPF18	-0.851333333	-0.17	0.020964327	0.681333333
TNKS1BP1	0.331333333	0.967666667	0.002651125	0.636333333
TRIB1	0.087	0.709	0.032804047	0.622
ONECUT2	0.402	1.008666667	0.02261418	0.606666667
CCT6A	-1.743333333	-1.225333333	0.007401735	0.518
COMMD1	-1.832666667	-1.379666667	0.034976118	0.453
COPS3	0.893666667	1.333333333	0.000957949	0.439666667
PDE7A	-0.724666667	-0.285333333	0.015073112	0.439333333
EIF2B5	0.168666667	0.591333333	0.014744277	0.422666667
TIMELESS	-0.907333333	-0.487333333	0.045342768	0.42
STRA13	-0.315333333	0.102	0.04673686	0.417333333
ADSL	-0.326	0.083333333	0.039375916	0.409333333
POLA2	-0.175	0.221	0.016811612	0.396
SIP1	-0.697	-0.321	0.02408634	0.376
LRFN4	-0.872	-0.498333333	0.046242021	0.373666667
RPN2	-0.154	0.201666667	0.021199361	0.355666667
STRBP	0.036666667	0.388	0.032901347	0.351333333
INCENP	-2.337333333	-2.023	0.049530855	0.314333333
AACS	-1.118666667	-0.826	0.030866114	0.292666667
SEPHS1	-1.733333333	-1.450666667	0.019625008	0.282666667
CHEK2	0.488666667	0.766333333	0.03952613	0.277666667
CLNS1A	-0.431666667	-0.171666667	0.043820346	0.26
IL27RA	0.454	0.651666667	0.029789901	0.197666667

Table S3. Functional enrichment (ToppGene) of WDHD1 binding partners identified via IP-MS.

Pathways	Number of shared proteins	-log10 (p-value)	Hit Count in Query List
Translation	6	4.276134036	RPL35A,EIF2S3,RPS6,RPS16,EIF3B,SEC61A1
MAP00640 Propanoate metabolism	3	4.159392121	ACAT1,ALDH3A2,MMUT
Formation of the ternary complex, and subsequently, the 43S complex	4	4.144723196	EIF2S3,RPS6,RPS16,EIF3B
GTP hydrolysis and joining of the 60S ribosomal subunit	5	3.92628165	RPL35A,EIF2S3,RPS6,RPS16,EIF3B
L13a-mediated translational silencing of Ceruloplasmin expression	5	3.92628165	RPL35A,EIF2S3,RPS6,RPS16,EIF3B
Ribosomal scanning and start codon recognition	4	3.912928794	EIF2S3,RPS6,RPS16,EIF3B
Translation initiation complex formation	4	3.886390849	EIF2S3,RPS6,RPS16,EIF3B
Activation of the mRNA upon binding of the cap-binding complex and eIFs, and subsequent binding to 43S	4	3.860120914	EIF2S3,RPS6,RPS16,EIF3B
Cap-dependent Translation Initiation	5	3.793174124	RPL35A,EIF2S3,RPS6,RPS16,EIF3B
Eukaryotic Translation Initiation	5	3.793174124	RPL35A,EIF2S3,RPS6,RPS16,EIF3B
Gene Expression	18	3.67223251	PPP2R2A,H2BC15,RPL35A,MT-CO2,MARS1,EIF2S3,COX5B,RPS6,CBX3,RPS16,MSH2,EIF3B,NUP93,SEC61A1,MOV10,HNRNPL,HNRNPR,CPSF7
Propanoate metabolism	3	3.495665088	ACAT1,ALDH3A2,MMUT
lysine degradation	2	3.239652921	ACAT1,ALDH3A2
Valine, leucine and isoleucine degradation	3	3.124186611	ACAT1,ALDH3A2,MMUT
Formation of a pool of free 40S subunits	4	3.032545632	RPL35A,RPS6,RPS16,EIF3B
Valine, leucine and isoleucine degradation	3	3.013273041	ACAT1,ALDH3A2,MMUT
Propanoate Metabolism	2	2.979638717	ACAT1,MMUT